 Q. J. R. Meteorol. Soc. 142: 2562–2578, July 2016 B DOI:10.1002/qj.2847

RMetS
Royal Meteorological Society

Impacts of in-canyon vegetation and canyon aspect ratio on the thermal environment of street canyons: numerical investigation using a coupled WRF-VUCM model

Sang-Hyun Lee,[a]* Hyunho Lee,[b] Seung-Bu Park,[b,c] Ju-Wan Woo,[a] Doo-Il Lee[a] and Jong-Jin Baik[b]
[a]*Department of Atmospheric Science, Kongju National University, Gongju, South Korea*
[b]*School of Earth and Environmental Sciences, Seoul National University, South Korea*
[c]*Department of Earth and Environmental Engineering, Columbia University, New York, NY, USA*

*Correspondence to: S.-H. Lee, Department of Atmospheric Science, Kongju National University, 56 Gongjudaehak-ro, Gongju 314-701, South Korea. E-mail: sanghyun@kongju.ac.kr

The thermal environment of an urban street canyon in summer becomes a great concern for human health under rapid urbanization. For accurate prediction of the in-canyon thermal environment, a realistic representation is required of microscale physical processes within the canyon as well as multi-scale atmospheric interaction between the canopy air and the overlying urban boundary layer. To accomplish this, the Vegetated Urban Canopy Model (VUCM), which interactively parametrizes in-canyon radiative/dynamic/thermodynamic/hydrological processes based on a combined framework of the two-dimensional single canyon and the single tree canopy, is implemented into the Weather Research and Forecasting (WRF) model. Using the coupled WRF-VUCM model, a series of simulations is performed for a hot summer day with a finest grid resolution of 0.333 km to investigate the impacts of in-canyon vegetation (permeable grass/soil surfaces and trees, with the vegatation fraction f_v ranging from 0 to 0.4 which corresponds to 0 to 15% in urban patch area) and canyon aspect ratio (h/w; ranging from 0.5 to 2) on the thermal environment of urban street canyons over the Seoul metropolitan area. The model simulation compares well with the measured 2 m temperatures (above zero-plane displacement height) and canopy air temperatures at 13 urban sites in Seoul, with root mean square errors of 1.0 and 0.96 °C, respectively. The increase of the in-canyon vegetation from 0 to 15% (at $h/w = 1$) leads to a reduction of the canopy air temperature throughout the diurnal cycle, exhibiting relatively larger cooling effect during daytime (∼1.1 °C on average) than at night (∼0.8 °C on average) under a limited condition for evapotranspiration by the in-canyon vegetation. Provided that the soil moisture is enough for the hydrological effect, the cooling effects significantly increase by a factor of ∼2.5 in both daytime and night-time. The increase of h/w from 0.5 to 2 (at $f_v = 0.2$) reduces the daytime canopy air temperature (∼1.3 °C on average) but increases the nocturnal canopy air temperature (∼0.3 °C on average). It is also found that the existence of in-canyon vegetation at $h/w > 1$ has a synergic cooling benefit to the thermal environment of street canyons compared to the effects of no vegetation. These results demonstrate the importance of interactive parametrization of the physical processes and the interplay of in-canyon vegetation and building density (via canyon aspect ratio) effects on accurate prediction of the thermal environment of urban street canyons.

Key Words: canyon aspect ratio; canopy air temperature; in-canyon vegetation; street canyon; Vegetated Urban Canopy Model (VUCM); WRF model

Received 18 August 2015; Revised 20 May 2016; Accepted 25 May 2016; Published online in Wiley Online Library 20 July 2016

1. Introduction

Urbanization is rapidly progressing in many countries over the world (Schneider *et al.*, 2015), and urban population is increasing in parallel with cities' expansion (Grimm *et al.*, 2008; Montgomery, 2008; UN, 2012). The aggregating trend in population is projected to accelerate in the future (UN, 2012). Consequently, more attention is paid to reducing adverse meteorological and environmental impacts (e.g. heat waves, air pollution) associated with rapid urban growth. Meanwhile, modern cities have morphological diversity (Stewart and Oke, 2012), which leads to diverse spatial and temporal variability in thermal environment of urban street canyons as well as so-called urban heat islands (UHIs).

To explicitly represent the urban morphological diversity and associated physical processes, urban canopy models (UCMs) have been developed for use in mesoscale meteorological modelling since the early 2000s (e.g. Masson, 2000; Kusaka *et al.*, 2001; Martilli *et al.*, 2002; Dupont and Mestayer, 2006; Lee and Park, 2008; Oleson *et al.*, 2008; Porson *et al.*, 2010; Lee, 2011; Ryu *et al.*, 2011). Many successful simulations demonstrating the UCMs' capability have been reported in performance in comparison with traditional land-surface models (e.g. Chen *et al.*, 2011; Lee *et al.*, 2011; Kusaka *et al.*, 2012). Recently, the UCMs have been widely applied to investigate physical processes in the urban boundary layer (e.g. Krayenhoff and Voogt, 2010; Lee and Baik, 2011; Loughner *et al.*, 2012; Li and Bou-Zeid, 2014; Wouters *et al.*, 2015) and to develop reliable strategies for sustainable cities (e.g. Li and Bou-Zeid, 2013; Martilli, 2014; Masson *et al.*, 2014; Li and Norford, 2016).

The recent international urban model comparison study evaluated various UCMs' ability in simulating urban surface energy balance fluxes and concluded with emphasizing the importance of physical parameterization of urban vegetation and accurate representation of urban morphological parameters (Grimmond *et al.*, 2010, 2011; Best and Grimmond, 2015). Many UCMs participated in the international comparison study considered no vegetation within an urban area or take urban vegetation into account using a tile (or mosaic) approach if urban vegetation exists. The tile approach has been used in mesoscale and global-scale models to represent land-cover heterogeneity in each model grid cell (Avissar and Pielke, 1989). Recently, the UCMs have been further developed by explicitly representing in-canyon vegetation (permeable grass/soil surfaces and/or trees) and thermal heterogeneity within an urban street canyon (e.g. Lee and Park, 2008; Lee, 2011; Lemonsu *et al.*, 2012; Loughner *et al.*, 2012; Wang *et al.*, 2013; Krayenhoff *et al.*, 2015; Ryu *et al.*, 2015; Yang *et al.*, 2015). These studies make use of different modelling approaches in the representation of in-canyon vegetation and parametrization of the associated physical processes. The Vegetated Urban Canopy Model (VUCM) by Lee and Park (2008) first introduces physically interactive parametrization of urban vegetation (soil surfaces and trees) with artificial surfaces (roofs, walls, and roads) among the UCMs using a combined framework of the single urban canyon (Oke, 1988) and the single tree canopy. Based on the single tree canopy concept introduced in the study, complicate morphology of urban trees is simply represented by the single tree canopy with a leaf area density profile, and the associated in-canyon physical processes are parametrized in an interactive way for use in a mesoscale atmospheric modelling. Lee (2011) further develops the VUCM by including the grass-covered soil surface parametrization within the canyon and demonstrates the model's performance in simulating the in-canyon micrometeorology as well as the surface energy balance fluxes. Loughner *et al.* (2012) adapts the single tree canopy concept to include urban tree parametrization in the single-layer UCM in WRF. Lemonsu *et al.* (2012) introduces a numerically efficient method to simulate in-canyon vegetation effects, in which the land-surface model applied for natural land-use grid cells is re-used for a vegetated surface fraction within the canyon. Wang *et al.* (2013) improves the single-layer UCM in WRF to represent thermal and hydrological heterogeneities at the roof, wall, and canyon surfaces including the urban greenery surface parametrization. However, urban tree effects are not parametrized in their study. Krayenhoff *et al.* (2015) represents urban trees within street canyons and above rooftops using a leaf area density profile and parametrizes the associated physical processes for the multi-layer UCM (Salamanca and Martilli, 2010). Ryu *et al.* (2015) includes urban tree parametrization in the single-layer UCM (Kusaka *et al.*, 2001; Wang *et al.*, 2013) using a similar representation method commonly used in microscale models. The recent development in the UCMs pursues more realistic representation of the urban vegetation and associated physical processes in a physically interactive parametrization framework.

Meanwhile, in-canyon vegetation (e.g. grasses, trees) and building morphology/arrangement have been recognized as important controlling factors of the UHI and outdoor thermal comfort in many numerical modelling and field measurement studies (e.g. Souch and Souch, 1993; Kunkel *et al.*, 1996; Taha, 1997; Ali-Toudert and Mayer, 2006; Giridharan *et al.*, 2008; Niachou *et al.*, 2008; Sugawara *et al.*, 2008; Shashua-Bar *et al.*, 2010; Ng *et al.*, 2012). The previous studies based on field measurements give good evidences for the effects of urban vegetation and buildings (e.g. Giridharan *et al.*, 2008; Sugawara *et al.*, 2008; Dimoudi *et al.*, 2013; Giovannini *et al.*, 2013), but they have a limitation in that many urban physical processes controlling the urban micrometeorology are hardly discriminated from measured variables. Meanwhile, numerical models can explicitly represent meteorological variables and physical processes based on the physical conservation laws, thus they can give an opportunity to understand the separate impacts of urban physical processes. In this context, a microscale numerical model that represent realistic urban morphological features and associated physical processes has been widely used to understand the controlling factors in the thermal environment of urban street canyons (e.g. Ali-Toudert and Mayer, 2006; Alexandri and Jones, 2008; Ng *et al.*, 2012). Despite the advantage of the microscale model against field measurements, the model's application is limited spatially to the building scale ($\sim 10-10^2$ m) due to intensive computing resource for a city-scale ($\sim 10^3-10^4$ m) application. On the other hand, a mesoscale atmospheric model can be applicable at a city scale with less computational cost, but previous mesoscale modelling studies have mainly focused on the UHI in the urban boundary layer (e.g. Chen *et al.*, 2011; Lee *et al.*, 2011; Kusaka *et al.*, 2012). Relatively little attention has been paid to the model's application to the thermal environment of urban street canyons due to a lack of physical parametrization of the urban physical processes, especially those hydrological processes relevant to urban vegetation (e.g. Taha, 1997; Li and Norford, 2016). The thermal environment of urban street canyons is actually controlled not only by the building-scale physical processes (e.g. in-canyon radiation transfer, heat convection and conduction at the artificial building surfaces, evapotranspiration by the urban vegetation) but also by the multi-scale atmospheric interaction of the canopy air with the overlying urban boundary layer. Therefore, the implementation of microscale urban physical process parametrization into a mesoscale atmospheric model is prerequisite for an accurate simulation of the in-canyon thermal environment at the city scale.

In this study, we aim to investigate the impacts of in-canyon vegetation (grass/soil surfaces and trees) and canyon aspect ratio on the street-level thermal environment over the Seoul metropolitan area, South Korea. In doing so, an integrated atmospheric modelling system is developed by implementing the VUCM into the mesoscale atmospheric model WRF (Weather Research and Forecasting). The WRF-VUCM can represent building-scale physical processes through physically interactive parametrization as well as multi-scale meteorological variations and interaction of the canopy air with the overlying urban

boundary layer. The fine-scale three-dimensional simulation using the coupled WRF-VUCM model can give a good opportunity for better understanding the impacts of in-canyon vegetation and canyon aspect ratio on the thermal environment of street canyons over urban areas, which is hardly accomplished in a microscale modelling. The remainder of this article is structured as follows. Section 2 describes the VUCM and the integrated atmospheric modelling system WRF-VUCM, and section 3 describes the experimental set-up and observations used for model validation. Section 4 presents model validation and fine-scale simulation results for the impacts of in-canyon vegetation and canyon aspect ratio on the thermal environment of urban street canyons. A summary and conclusions follows in section 5.

2. Model description

2.1. The Vegetated Urban Canopy Model (VUCM)

The VUCM is an urban land-surface model developed for the use of mesoscale meteorological and environmental modelling, which is a physically interactive scheme between the artificial surfaces (roof, wall, road) and natural surfaces (grass, soil, tree) within an urban canyon so that the urban geometry and associated physical processes are represented in a more realistic manner (Lee and Park, 2008; Lee, 2011). The urban geometry in the model is represented by the roof width (R), canyon width (W) and the building height (H_{building}) based on the single canyon concept (Oke, 1988), and the roof (f_R) and canyon (f_C) fraction. The in-canyon vegetation (f_v) is composed of the vegetated grass/soil surfaces and urban trees. The vegetated grass/soil surfaces (f_v), which consist of the grass-covered surface (f_{grs}) and the bare soil surface (f_s), take a fraction of the canyon width, while the morphology of the urban trees is represented as a single tree canopy that is characterized by the planar coverage fraction of urban trees (f_{tree}), the mean tree height (H_{tree}), and the mean leaf area index (LAI_{tree}) with a leaf area density profile (Figure 1). Based on the morphological representation, the energy and moisture conservation laws are applied on each surface to calculate short-wave/long-wave radiative fluxes and turbulent heat and moisture fluxes at the roof and canyon top, for which various urban physical processes (e.g. short-wave/long-wave radiative transfer, turbulent heat and moisture exchanges, heat and moisture conduction) are parametrized. The momentum drag by the building and the tree canopy is included in a simple relation. The urban tree canopy is explicitly represented as an energy-exchanging medium in the physical processes. More descriptions of the VUCM are given in the Appendix A.

2.2. Integrated atmospheric modelling system WRF-VUCM

The WRF model is a three-dimensional meteorological model with a fully compressible and non-hydrostatic dynamic core, including various physical parametrizations of short-wave/long-wave radiation, atmospheric boundary-layer turbulence, grid-resolved microphysics, sub-grid clouds, and land-atmosphere exchange processes (Skamarock *et al.*, 2008). It has been widely used for various meteorological and environmental applications. In this study, the VUCM by Lee (2011), an updated version of Lee and Park (2008), is implemented in the WRF model version 3.6.1 for development of an integrated atmospheric modelling system WRF-VUCM. In the WRF model, the Noah land-surface scheme (as an option) calculates surface-layer turbulent fluxes of momentum, heat, and moisture and upward short-wave/long-wave radiative fluxes (in the form of albedo and surface skin temperature) for each grid cell (Chen and Dudhia, 2001). The turbulent and radiative fluxes are used as bottom boundary conditions of the WRF model's governing equation set. In the coupled WRF-VUCM model, the VUCM and the Noah land-surface model calculate the surface-layer turbulent and radiative fluxes for urban grid cells and non-urban grid cells, respectively. The meteorological forcing required for driving the VUCM and the Noah land-surface scheme are provided by the WRF variables predicted at the model's first vertical level (Figure 1). Thus, the VUCM provides the boundary condition of the WRF model for the urban grid cells. This VUCM implementation into the WRF model allows the canopy air to interact with multi-scale atmospheric motions at the overlying atmosphere and the roof surface in terms of the turbulent and radiative exchanges.

The WRF-VUCM model includes three urban categories of the commercial/industrial area, high-density residential area, and low-density residential area following the default WRF-UCMs. Each urban grid cell is designated as one of the urban types, and it is subsequently represented by an urbanized area patch and a non-urban area patch with their coverage fraction ('*tile*' representation). Therefore, the turbulent and radiative fluxes of the urban grid cell are calculated as weight-averaged fluxes of the urban patch calculated by the VUCM and the non-urban patch calculated by the Noah land-surface model as:

$$\overline{F}_{\text{urban}} = f_{\text{urban}} F_{\text{urban}} + (1 - f_{\text{urban}}) F_{\text{non-urban}}, \tag{1}$$

where $\overline{F}_{urban}$ is the grid-cell averaged turbulent and radiative fluxes, F_{urban} and $F_{\text{non-urban}}$ are the turbulent and radiative fluxes for the urban patch (by the VUCM) and the non-urban patch (by Noah land-surface model), respectively, and f_{urban} is the urbanized area fraction in a grid cell. Subsequently, the turbulent and radiative fluxes of the urbanized area patch (F_{urban}) are calculated in the VUCM as:

$$F_{\text{urban}} = f_R F_{\text{roof}} + (1 - f_R) F_{\text{canyon}}, \tag{2}$$

where F_{roof} and F_{canyon} are the turbulent and radiative fluxes at the roof surface and the canyon top, respectively. The energy fluxes at the roof (F_{roof}) and the canyon top (F_{canyon}) have no interaction with each other in a stand-alone version of the VUCM.

Meanwhile, the canopy air temperature (T_C) within the urban street canyon is a prognostic variable in the WRF-VUCM model, which is calculated based on the thermodynamic energy conservation law as (Lee and Park, 2008; Lee, 2011):

$$\rho c_p \Delta V_C \frac{dT_C}{dt} = \left[\frac{2h}{w} H_w + f_r H_r + f_v H_v + \sigma_l H_l + H_{AH} - H_C \right] \times \Delta A_C. \tag{3}$$

Here, H_w, H_r, $H_v (= f_s H_s + f_{\text{grs}} H_{\text{grs}})$, and H_l are the sensible heat fluxes (W m^{-2}) at the wall, road, and vegetated (grass/soil) surfaces, and the tree canopy, respectively; H_C is the sensible heat flux at the canyon top; H_{AH} is the anthropogenic heat flux released within the street canyon; ΔV_C and ΔA_C are the volume of the canopy air (m^3) and the canyon bottom area (m^2), respectively; σ_l is the leaf aspect ratio (Lee and Park, 2008) which is used to convert the energy fluxes at the tree canopy into the equivalent fluxes to the horizontal canyon floor; ρ is the air density; c_p is the specific heat capacity of dry air. The 2 m potential temperature ($\theta_{2\text{m}}$) for the urban patch is diagnosed using the Monin-Obukhov similarity theory (Theeuwes *et al.*, 2014):

$$\theta_{2m} = \theta^{atm} - \frac{\theta_{*,U}}{k} \left[\ln\left(\frac{z-d}{2}\right) - \psi_h\left(\frac{z-d}{L}\right) + \psi_h\left(\frac{2}{L}\right) \right], \tag{4}$$

where $\theta_{2\text{m}} (= T_{2m}(p_0/p)^{R/c_p})$ is defined at the 2 m height above zero-plane displacement height (d) of the urban patch; θ^{atm} is the potential temperature at the reference level (the model's first half-sigma level); $\theta_{*,U}$ is the potential temperature characteristic scale for the urban patch; k is the von Kármán constant (=0.4); L

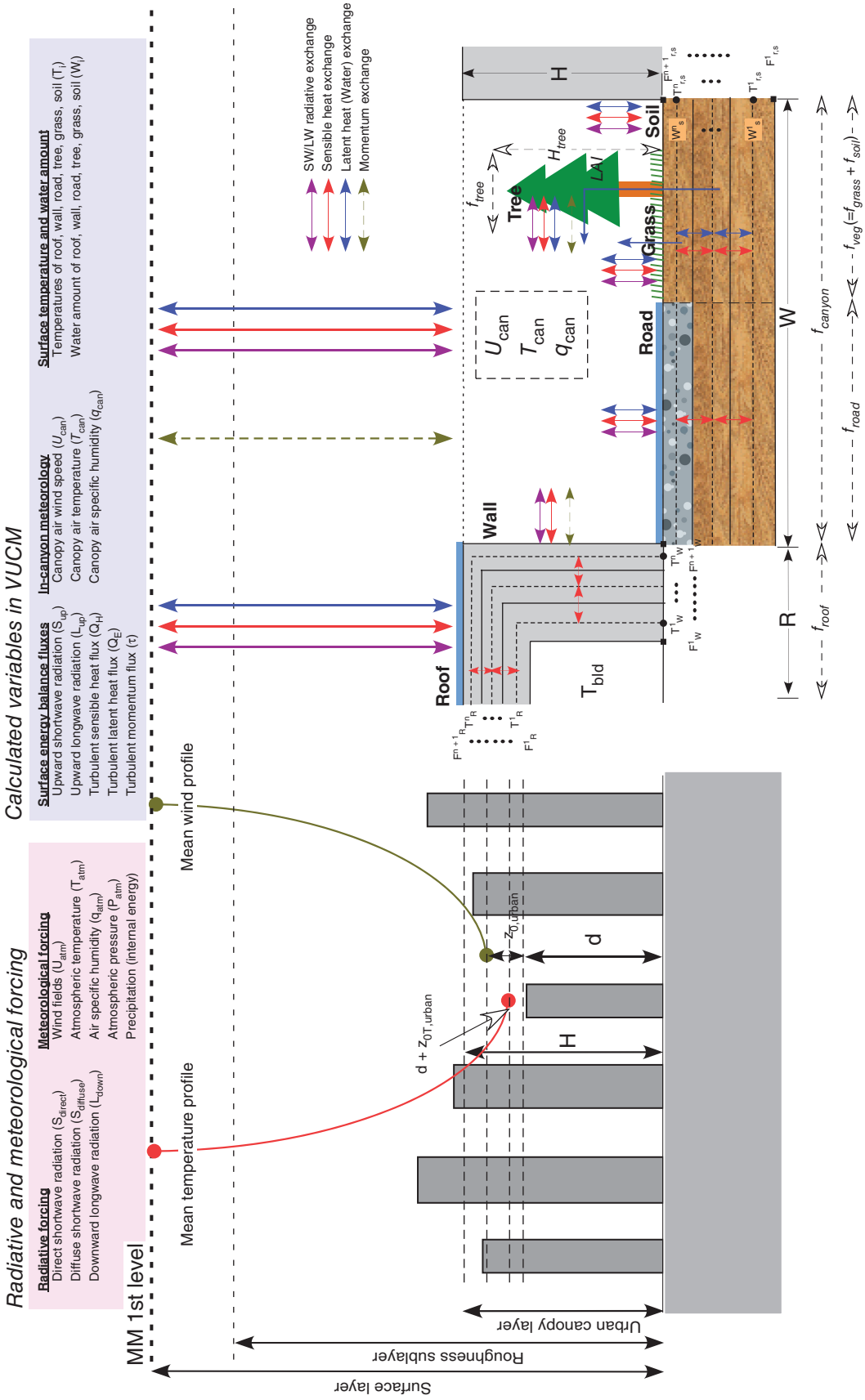

Figure 1. Schematic diagrams of the VUCM (right) and its coupling with a meteorological model (left) (modified from Lee and Park, 2008; Lee, 2011). In the left panel, H, d, z_0, and z_{0T} are the mean building height, zero-plane displacement height, roughness length for momentum, and roughness length for heat, respectively. In the right panel, F denotes the heat and/or moisture fluxes at each surface layer and T and W are the temperature and moisture amount at each surface layer. Subscripts R, w, r, s, and grs represent roof, wall, road, soil, and grass surfaces, respectively.

is the Obukhov length-scale. ψ_h is the integrated stability function for heat transfer, which is expressed as (Högström, 1996)

$$\psi_h\left(\frac{z}{L}\right) = \begin{cases} 2\ln\left(\frac{1+\left(1-16\frac{z}{L}\right)^{1/2}}{2}\right) & for\ \frac{z}{L} < 0 \\ -5\frac{z}{L} & for\ \frac{z}{L} \geq 0 \end{cases}. \quad (5)$$

The canopy air temperature (T_C) and 2 m air temperature (T_{2m}) are popular indicative variables used to quantify the urban heat island intensity and the thermal discomfort. In highly built-up urban areas, the thermal environment at rooftop levels can be distinguished from that in street canyons due to high values of d. The coupled WRF-VUCM model explicitly defines the urban canopy layer as a single atmospheric layer, thus T_C is used to predict the thermal environment of urban street canyons (Figure 1). The use of 2 m temperature above ground level, which may be diagnosed based on the surface-layer similarity theory, has a limitation to accurately quantify the thermal environment of urban street canyons in that the complicated in-canyon physical processes are not directly described, except that the similarity theory will not be valid in a region below d.

3. Experimental set-up

3.1. *The WRF-VUCM model set-up*

To investigate the impacts of in-canyon vegetation and canyon aspect ratio on the thermal environment of street canyons over the Seoul metropolitan area, the WRF-VUCM model is configured with five two-way interactive domains using horizontal grid spacing (mesh) of 27 km (107 × 107), 9 km (81 × 81), 3 km (69 × 69), 1 km (105 × 93), and 0.333 km (189 × 159). The coarsest domain covers eastern China, the Korean peninsula, and western Japan (Figure 2), while the finest domain covers the Seoul metropolitan area. All the model domains are configured with 43 vertical layers. The vertical grid spacing is variable with ~35 m depth in the lowest model layer, and the model-top height is ~26.5 km (20 hPa). The physical parametrizations used for simulations are the Dudhia short-wave radiation (Dudhia, 1989), the Rapid Radiative Transfer Model for long-wave radiation (Mlawer *et al.*, 1997), the YSU turbulence scheme (Hong *et al.*, 2006), the modified MM5 surface-layer similarity scheme (Jimenez *et al.*, 2012), the WRF single-moment six-class microphysics scheme (Hong and Lim, 2006), the Kain-Fritsch cumulus parametrization (Kain, 2004), and the Noah land-surface model (Chen and Dudhia, 2001) for natural land-use grid patches. These physical parametrizations are used identically in all the model domains except for the cumulus parametrization applied only for domains 1 and 2. In the model configuration, the effective resolution of the finest domain ($\Delta X = 0.333$ km) is estimated as ~2 km according to Skamarock (2004). Thus, the convective boundary-layer turbulence may be partly resolved in the grid-scale, falling in the 'terra incognita' or 'grey zone' (Wyngaard, 2004). To fully represent the turbulence transport of heat by the resolved and parametrized turbulence in the convective boundary-layer regime, the use of the turbulence scheme is needed even for the WRF simulation with the fine-grid resolution (Shin and Dudhia, 2016).

For urban grid cells, the VUCM is used to compute the WRF model's bottom boundary conditions through calculation of the land-atmosphere exchange processes. The urban grid cells are precisely represented using high-resolution (30 m) land-use data produced by the Korea Environmental Administration. The urbanized areas over the Seoul metropolitan area are mostly classified as high-density residential (84%) with a small fraction of industrial/commercial (16%) (Figure 2(b)). Each urban grid cell in the domain is assigned to consist of 95% built-up surface and 5% natural surface ('*tile*' representation). The urbanized area patch, which is handled by the VUCM, is composed of the building fraction (f_R) and street canyon fraction (f_C), each taking

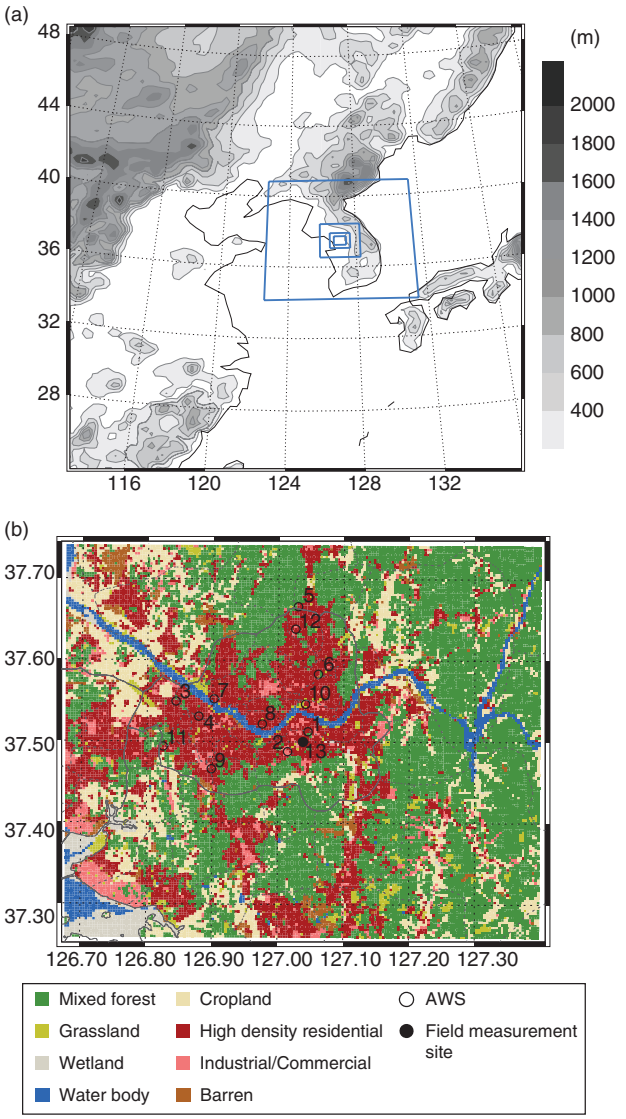

Figure 2. (a) WRF model domains. The inner boxes indicate nested domains, and shaded contours denote topography. (b) Spatial distribution of dominant land-use types in the innermost domain 5. The numbers indicates locations of the surface meteorological sites (○) operated by the Korean Meteorological Administration and a field measurement site (●) located in a high-rise building district.

50%. The street canyon (f_C) is subdivided by the artificial road surface (f_r, 80%) and in-canyon vegetated grass/soil surfaces (f_v, 20%). The in-canyon vegetated surfaces are assigned to consist of 70% of grass-covered surface (f_{grs}) and 30% bare soil (f_s). The tree canopy (f_{tree}) is assigned as 14% of the street canyon fraction. The mean building height and tree canopy height are assigned as 12 and 7.5 m, respectively, with a canyon aspect ratio (h/w) of 1 in the base simulation. The aerodynamic roughness lengths for momentum and heat, heat conductivity and capacity of buildings, and radiative properties (albedo and emissivity) of the artificial and natural surfaces are assigned based on previous modelling studies for the Seoul metropolitan area (e.g. Lee and Baik, 2011; Ryu and Baik, 2013). The anthropogenic heat is included for the urban patch with a daily maximum value of 45 W m^{-2} based on Lee and Kim (2015), and the diurnal profile of the anthropogenic heat is same as in the default profile of the WRF model (Chen *et al.*, 2011). The leaf area index values assigned for the tree canopy and the grass surfaces are 6 and 2, respectively. The soil texture is assigned as a sandy clay type and the soil moisture amount is initially assigned as 50% (0.21 m^3 m^{-3}) of its saturation value in the base simulation, in which evapotranspiration by the in-canyon vegetation is significantly suppressed. Table 1 summarizes the model parameters used in the simulations.

Table 1. The VUCM parameter values used for urban patches.

Parameter	Unit	Urban
Roof fraction (f_R)	–	0.5
Canyon fraction (f_C)	–	0.5
Road fraction (f_r)	–	0.8
Vegetated area fraction (f_v)	–	0.2[a]
Grass/soil surface fraction (f_{grs}/f_s)	–	0.7[a]/0.3[a]
Tree fraction (f_{tree})	–	0.14[a]
Mean building height ($H_{building}$, h_b)	m	12.0
Mean tree height (H_{tree}, h_f)	m	7.5
Mean canyon aspect ratio (h/w)	–	1.0[a]
Urban roughness lengths for momentum and heat(z_0, z_{0T})	m	1.2, 0.12
Roof roughness lengths for momentum and heat($z_{0,R}$,$z_{0T,R}$)	m	0.15, 0.0015
Road roughness lengths for momentum and heat($z_{0,r}$, $z_{0T,r}$)	m	0.05, 0.005
Roof albedo/emissivity (α_R/ε_R)	– / –	0.20/0.90
Wall albedo/emissivity (α_w/ε_w)	– / –	0.25/0.90
Road albedo/emissivity (α_r/ε_r)	– / –	0.10/0.94
Soil albedo/emissivity (α_s/ε_s)	– / –	Variable/0.98
Tree albedo/emissivity ($\alpha_{tree}/\varepsilon_{tree}$)	– / –	0.20/0.96
Grass albedo/emissivity ($\alpha_{grs}/\varepsilon_{grs}$)	– / –	0.20/0.95
Roof thermal conductivity (k_R)	$W\,m^{-1}\,K^{-1}$	0.90
Wall thermal conductivity (k_w)	$W\,m^{-1}\,K^{-1}$	0.80
Road thermal conductivity (k_r)	$W\,m^{-1}\,K^{-1}$	0.80
Roof volumetric heat capacity (C_R)	$MJ\,m^{-3}\,K^{-1}$	1.4
Wall volumetric heat capacity (C_w)	$MJ\,m^{-3}\,K^{-1}$	1.5
Road volumetric heat capacity (C_r)	$MJ\,m^{-3}\,K^{-1}$	1.7
Soil texture	–	Sandy clay
Leaf area index for tree (LAI_{tree})	–	6.0
Leaf area index for grass (LAI_{grs})	–	2.0
Initial soil moisture	$m^3\,m^{-3}$	0.21[a]

[a]These values are changed in the sensitivity simulations.

The selected simulation case is a hot summer day (25 June 2013) when the maximum 2 m temperature was 30.3 °C at an urban site with a mean relative humidity of ∼60% under a synoptic high-pressure system. During the day, a high surface ozone level (∼115 ppbv) was also recorded at a high-rise building site in Seoul (Park *et al.*, 2015). The WRF-VUCM simulation is performed for 3 days from 0000 UTC (0900 LST) 23 June 2013 to 0000 UTC 26 June 2013 using meteorological initial/boundary condition from the National Centers for Environmental Prediction (NCEP) final analysis data (FNL) (horizontal resolution of 1° × 1°; time intervals of 6 h), and the first 39 h is used for the model spin-up. The FNL data have resolved the evolution of the synoptic high-pressure system that influenced the study area during the period of interest. Along with the base simulation, additional sensitivity simulations are performed to investigate the impact of changes to the in-canyon vegetation (grass/soil and tree) and canyon aspect ratio ($f_v = 0$, 0.1, 0.3, 0.4 and $h/w = 1/2$, 2/3, 3/2, 2). When f_v changes, the grass/soil surface fraction (f_{grs}/f_s) and the tree canopy fraction (f_{tree}) are simultaneously changed in proportion to f_v. When h/w changes, both the mean building height (h_b) and the canyon fraction (f_C) remain constant to represent the change of building density (or mean canyon width). The values of f_v and h/w are chosen from a ballpark estimation of spatial morphological variability within the Seoul metropolitan area. In addition, sensitivity simulations to soil moisture amount are also performed with the increased soil moisture of 75% of the saturation ($0.32\,m^3\,m^{-3}$) to examine the hydrological effects of the in-canyon vegetation on the thermal environment of street canyons.

3.2. Observations

The 13 urban meteorological sites located within Seoul are used to validate the model's performance in simulating near surface air temperature. Table 2 presents the location of measurement sites and morphological characteristics surrounding the urban sites. Among them, 12 meteorological sites are routinely operated by the Korea Meteorological Administration (KMA), and the 13th measurement site in Table 2 was temporally operated at street level in a high-rise building area (Park *et al.*, 2015). The temperature instruments installed at the KMA sites are mostly mounted ∼2 m above the rooftop of buildings ranging from 8 to 20 m above ground level, thus the observation represents the air temperature roughly around the mean building heights (h_b) that are estimated at 7–20 m above ground level from the high-resolution building information data. The installed temperature instruments are platinum resistance thermometers (PT-100) which are placed in an aluminum shelter to block radiation, and the forced ventilation method is adopted at all the sites following the World Meteorological Organization (WMO) guideline (Oke, 2006). The air temperature data are gathered at 1 min intervals with a sensor accuracy of ±0.3 °C, and the data quality is controlled by the KMA following the WMO recommendation (Zahumensky, 2004). On the other hand, the street-level measurement was conducted in the central business district in Seoul using a temperature probe (HMP155A, Vaisala) mounted on a tripod at 2 m above ground level. The sensor accuracy is ±0.2 °C and the data was recorded at 1 min intervals through a data logger (CR1000, Campbell Scientific).

4. Results and discussion

4.1. Model validation

The performance of the WRF-VUCM model in simulating near-surface thermal environment is validated using the observed near-surface air temperatures at the 13 urban meteorological sites (Table 2). Here, the 2 m temperatures obtained at the 12 KMA sites are used to evaluate the model's diagnostic 2 m temperatures (above zero-plane displacement height d), while the in-canyon air temperatures obtained at a high-rise building site are used to evaluate the model-predicted canopy air temperatures. The observed and simulated temperatures are averaged over 1 h intervals for comparison. The simulated 2 m temperature and canopy air temperature are from the nearest grid cell to the measurement location without any spatial interpolation between model grids.

Table 2. Morphological characteristics of the urban meteorological sites used in the model validation.

Site No.	Longitude (°E)	Latitude (°N)	h_{obs} (m)	h_b (m)	f_R (%)	$f_{\text{impervious}}$ (%)	f_{pervious} (%)	d (m)
1	127.047	37.513	11	12.9	63	29	8	9.0
2	127.016	37.489	11	13.8	50	40	10	9.7
3	126.843	37.550	11	13.0	33	40	27	9.1
4	126.878	37.530	5	19.3	24	63	13	13.5
5	127.030	37.666	14	8.0	43	55	2	5.6
6	127.060	37.585	14	6.5	49	31	20	4.6
7	126.903	37.552	8	7.6	42	43	15	5.3
8	126.976	37.520	14	11.2	31	48	21	7.8
9	126.900	37.466	14	7.7	61	38	1	5.4
10	127.039	37.547	17	7.0	20	45	35	4.9
11	126.827	37.494	14	7.7	36	42	22	5.4
12	127.026	37.640	20	8.5	61	37	2	6.0
13	127.038	37.500	2	20.2	44	51	5	14.1

Here h_{obs}, h_b, f_R, $f_{\text{impervious}}$, and f_{pervious} are the measurement (sensor) height, mean building height, building plan area fraction, impervious plan area fraction, and pervious plan area fraction. The morphological properties are estimated for urbanized areas within 400 × 400 m^2 following Stewart and Oke (2012). The zero-plane displacement height (d) is estimated using a relation of 0.7 h_b.

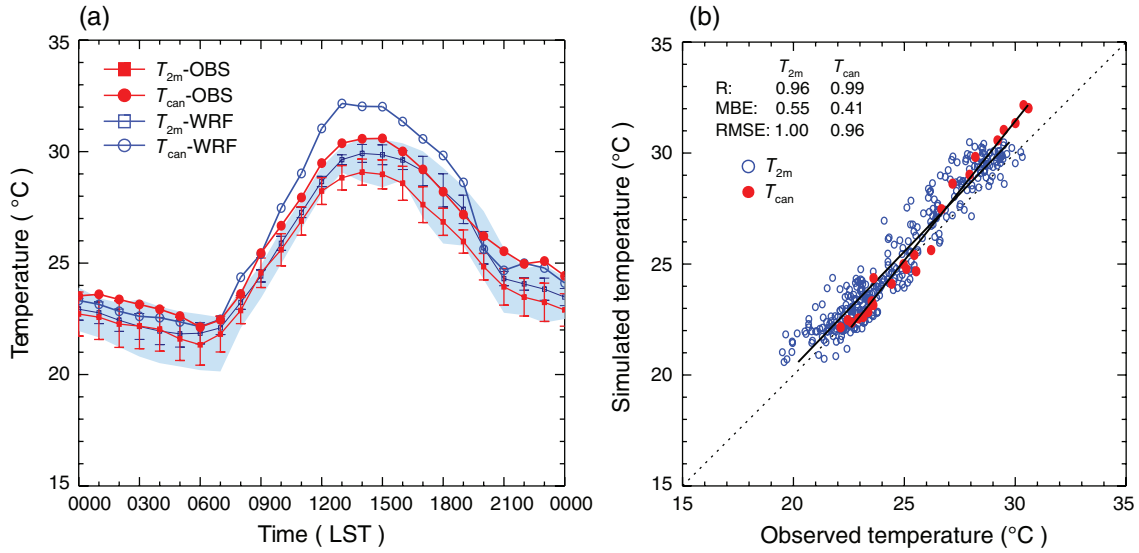

Figure 3. (a) Diurnal variations of the observed and simulated 2 m temperatures and the canopy air temperatures for 25 June 2013. Spatial (site) mean and standard deviation values (vertical bars) of the 12 urban sites are plotted for both the observed and simulated 2 m temperatures in the base simulation. The shaded area indicates the minimum-maximum range of the 2 m temperatures in all sensitivity simulations. (b) Scatterplot of the observed and simulated 2 m temperatures and the canopy air temperatures.

Figure 3 compares the observed and simulated 2 m temperatures and canopy air temperatures over the Seoul metropolitan area on 25 June 2013. The mean observed 2 m temperature on the hot summer day ranges from ∼21 °C at dawn to ∼29 °C around 1400 LST. The model simulation compares well with the observed 2 m temperature with a correlation coefficient (R) of 0.96, a mean bias error (MBE) of 0.55 °C, and a root mean square error ($RMSE$) of 1.0 °C. The spatial variability of the observed 2 m temperature is relatively large at night when the thermal influence of urban land-use and human activity is confined to a lower urban surface layer (e.g. Kim and Baik, 2005). The model falls short of fully reproducing the spatial variability in the observed 2 m temperature throughout the day. This is partly due to a simplified spatial representation of the urban morphological features (e.g. urban vegetation, building density). The sensitivity simulation results identify this fact to some extent, showing better agreement with the observed spatial variability (shaded area in Figure 3(a)). Therefore, more realistic representation of the urban morphology will be necessary for better simulation of the observed temperature and its spatial variation.

The observed canopy air temperature is higher by 1–2 °C than the mean observed 2 m temperatures measured at rooftop levels throughout the day. The temperature difference between the two levels is larger in the daytime (1–2 °C) than in the night-time (∼1 °C) (Figure 3(a)), and the temperature difference between the street level and the rooftop is also larger during daytime (∼1 °C with a maximum difference of ∼1.4 °C) than at night (0.2–0.8 °C) at the high-rise building area (Park *et al.*, 2015). These observations indicate that the diurnal amplitude of the canopy air temperature is larger than that at the rooftop level. The simulated canopy air temperature compares well with the observed temperature with $R = 0.99$, $MBE = 0.41$ °C, and $RMSE = 0.96$ °C. The simulated diurnal amplitude (∼10.0 °C) is slightly larger than that in the observation (∼8.5 °C), which leads to slight overestimation of the daytime temperature by 1–2 °C.

4.2. *Impacts of in-canyon vegetation and canyon aspect ratio*

The good performance of the WRF-VUCM model in simulating near-surface air temperature leads us to the sensitivity simulations to investigate the impacts of in-canyon vegetation (grass/soil surfaces and tree) and canyon aspect ratio on the in-canyon thermal environment. The assigned in-canyon vegetation fraction (f_v) values of 0, 0.1, 0.2, 0.3, and 0.4 represent 0, 3.8, 7.6, 11.4, and 15.2% of the urban grid cell. Meanwhile, the increase of canyon aspect ratio (h/w) values (1/2, 2/3, 1, 3/2, and 2) represents narrower canyon width (higher building density). Note that the base simulation is performed with $f_v = 0.2$ and $h/w = 1$ at a lower soil moisture condition (50% of saturation). The following analyses are made using the 13 urban grid cells nearest to the measurement sites in Table 2.

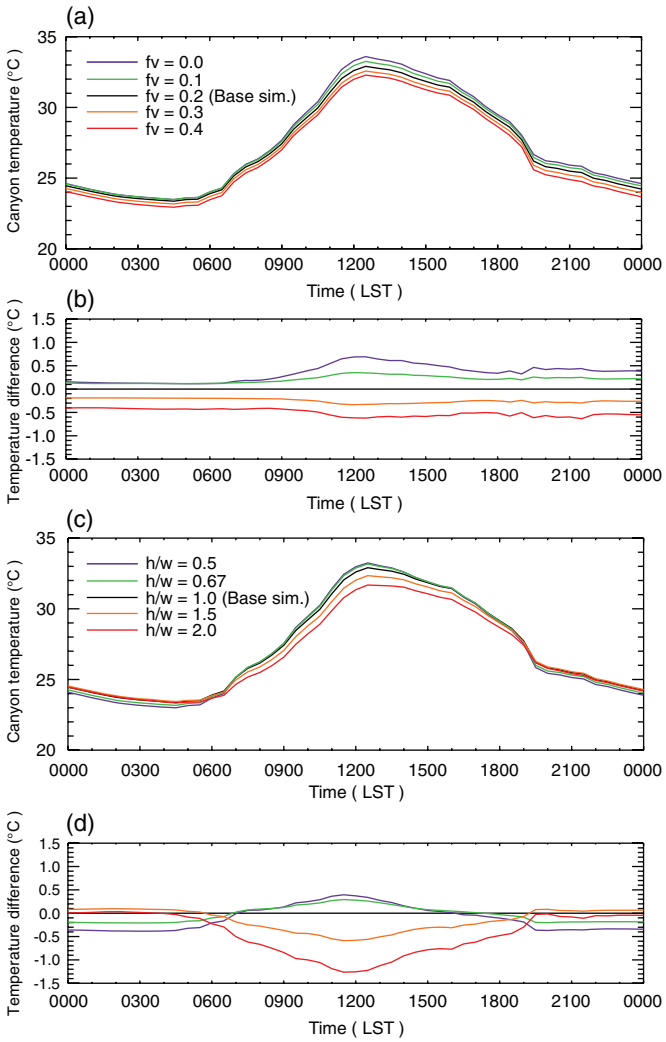

Figure 4. Diurnal variations of (a) the canopy air temperature and (b) the temperature difference from the base simulation for different in-canyon vegetation fractions. (c) and (d) are as (a) and (b) but for different canyon aspect ratios. The simulated canopy air temperatures are grid-averaged values over the 13 urban meteorological sites for 25 June 2013, and the temperature differences are defined as $T_C^{sens} - T_C^{base}$.

Figure 4 presents the diurnal variations of the canopy air temperatures in the simulations changing (a, b) the in-canyon vegetation and (c, d) the canyon aspect ratio. The canyon aspect ratio is fixed at 1 in the simulations changing f_v, while the in-canyon vegetation is fixed to 0.2 in the simulations changing h/w. The increase of in-canyon vegetation leads to a canopy air temperature reduction during the diurnal cycle, with a relatively larger cooling effect during daytime than at night. About 15% in-canyon vegetation of the urban grid cell reduces the daytime (night-time) temperature by ∼1.1 °C (∼0.8 °C) on average compared to no vegetation (Figure 4(b)). The vegetation cooling effects and the temporal trends compare well with the results found in field measurements over urban areas (e.g. Giridharan *et al.*, 2008) and microscale urban numerical modelling (e.g. Ng *et al.*, 2012), considering different geographical locations and seasons. Meanwhile, the increase of canyon aspect ratio tends to lower the canopy air temperature during daytime but enhances the nocturnal canopy air temperature. When increasing h/w from 0.5 to 2, the daytime canopy air temperature decreases by ∼1.3 °C on average but the night-time temperature increases by ∼0.3 °C in the diurnal cycle. The daytime cooling effect due to the change in h/w is comparable to that of the in-canyon vegetation effect, but their nocturnal thermal effects compensate each other for the temperature change.

Figure 5 compares the impacts of the in-canyon vegetation and the canyon aspect ratio on the canopy air temperatures at noon (1200 LST) and midnight (0000 LST) under different soil moisture conditions in the urban patches. In general, the soil moisture amount can control the hydrological activities of the in-canyon grass/soil surfaces as well as the tree canopy (e.g. Lee, 2011; Best and Grimmond, 2014). When the soil moisture amount is increased to 0.32 $m^3\ m^{-3}$ (75% of the saturation value) so that the evapotranspiration of the in-canyon vegetation ('hydrological effect') is more activated, the vegetation cooling effects increase to ∼3.0 °C at noon and ∼1.4 °C at midnight in increasing f_v from 0 to 0.4, which indicates the cooling effects are enhanced by a factor of ∼2.5 for both day and night compared to the lower soil moisture condition (Figure 5(a,b)). The enhanced hydrological cooling effects by the in-canyon vegetation are also clearly found at both noon (∼1.0 °C) and midnight (∼0.6 °C) in all the sensitivity simulations changing h/w (Figure 5(c,d)). Though the thermal effects of h/w are less sensitive to the soil moisture amount change for both day and night, the existence of the in-canyon vegetation plays an important role through nonlinear physical interaction. The combined effects of h/w with the in-canyon vegetation induce a synergic cooling of the canopy air temperature during daytime (∼0.7 °C) and at night (∼0.9 °C) compared to the no vegetation case. It is interesting that the in-canyon vegetation has cooling effects at both day and night even when the hydrological cooling effects are significantly suppressed, which is further discussed below. The simulations with no in-canyon vegetation (dashed line with circle in Figure 5(c,d)) that show a monotonically decreasing (increasing) trend in the canopy air temperature at noon (midnight) in terms of h/w compares quantitatively well with previous modelling studies (e.g. Ali-Toudert and Mayer, 2006; Marciotto *et al.*, 2010) which investigated the in-canyon thermal effects at different canyon aspect ratios with no vegetation. These results show that the impacts of h/w can be significantly modulated by the existence of in-canyon vegetation.

Figure 6 compares the simulated surface energy balance fluxes at the canyon top at noon (1200 LST) and midnight (0000 LST) as a function of in-canyon vegetation fraction and canyon aspect ratio under different soil moisture conditions. Figures 7 and 8 present the simulated surface temperatures of the wall and ground surfaces at noon and midnight for the sensitivity simulations. During daytime, the increase in f_v reduces net short-wave radiation as a result of the increased in-canyon surface albedo and the shading effect by the tree canopy. This indicates that the radiative effect by the increased surface albedo due to the tree canopy and the grass/soil surfaces is greater than the enhanced radiation trapping effect by the tree canopy. The reduced short-wave radiation decreases the wall and ground surface temperatures (Figure 7), which is related to a higher net long-wave radiation (lower long-wave emission from the in-canyon surfaces) and a decreased sensible heat flux due to atmospheric stability reduction between the canopy air and the overlying atmosphere (Lee, 2011). The short-wave radiative effects by the in-canyon vegetation are largely attributed to the radiative interaction of the tree canopy which is relatively tall compared to the building height. A similar increase in the effective short-wave albedo due to the in-canyon vegetation is also found by Krayenhoff *et al.* (2014), who demonstrated the enhanced short-wave albedo due to urban trees in a multi-layer modelling framework. Meanwhile, the increase in f_v can reduce the in-canyon wind speed ('dynamic effect by vegetation'), resulting in lower turbulent heat exchanges between the canopy air and the in-canyon wall/ground surfaces, reducing the sensible heat fluxes from the wall/ground surfaces during daytime. At night, the storage heat contributes to retarding the cooling of the canopy air (Oke, 1982), but the storage heat contribution decreases along with the sensible heat flux at the canyon top as f_v increases, which is in line with the decrease in the canopy air temperature (Figure 5).

On the other hand, the increase in h/w enhances the net short-wave and long-wave radiation during daytime due to the enhanced radiation trapping within the canyon (Figure 6), but the wall and ground surface temperatures decrease due to the increased wall

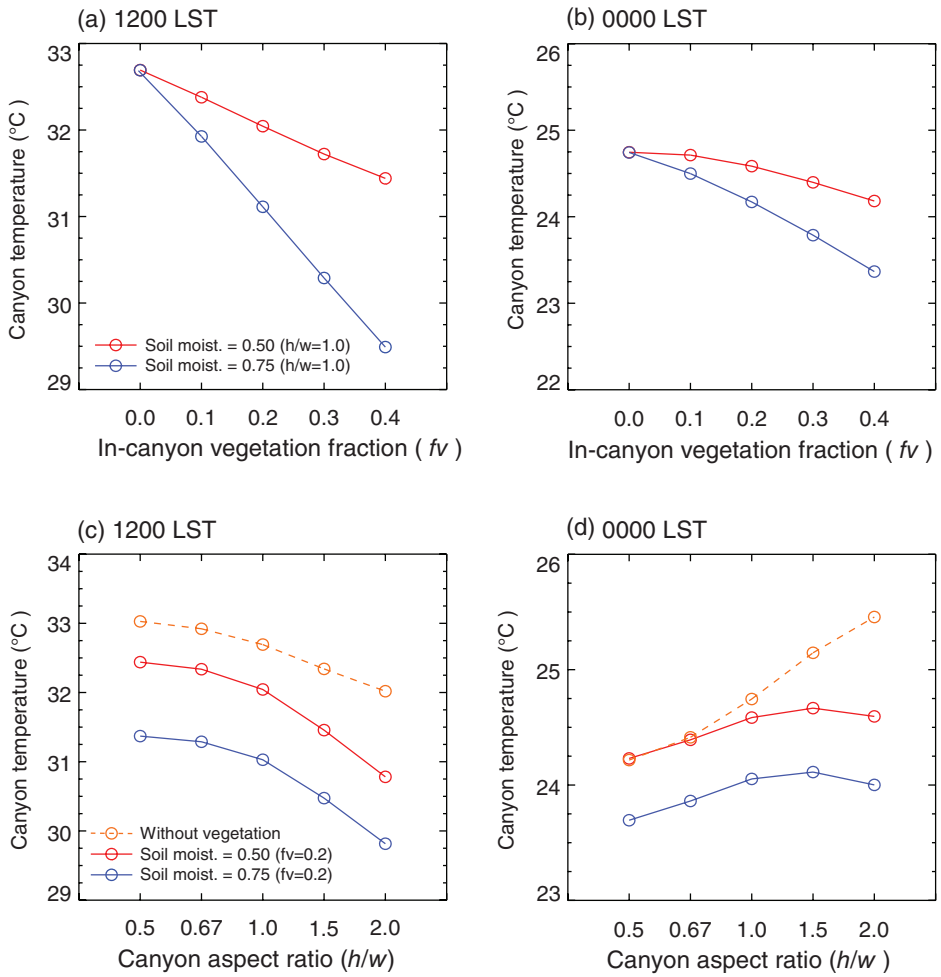

Figure 5. Canopy air temperatures at (a, c) noon (1200 LST) and (b, d) midnight (0000 LST) in the simulations versus (a, b) the in-canyon vegetation fraction and (c, d) the canyon aspect ratio. The soil moisture amount is represented by the ratio of the soil moisture assigned to the saturation value for the sandy clay texture. In (c) and (d), the dashed lines indicate the canopy air temperatures simulated without in-canyon vegetation.

surface areas and shading effects by the building and the tree canopy, respectively (Figure 8). The decrease of the sensible heat flux is attributed to the reduced surface temperatures and the reduced in-canyon wind speed. Note that the shading effect by the building represents partitioning of the incident solar radiation more into the wall surface than the ground surfaces keeping the energy conservation law, while the shading effect by the tree canopy represents partitioning of the incident solar radiation into the tree canopy absorption, reflection to the atmosphere, and the radiation reaching the wall and ground surfaces. At night, the storage heat plays an important role in the in-canyon surface energy balance, but the storage heat and the sensible heat fluxes tend to increase with h/w due to the long-wave radiation trapping effect (Figure 6).

In all the sensitivity simulations changing f_v and h/w, the increase of soil moisture amount enhances the hydrological effects of in-canyon vegetation, leading to decrease (increase) of the sensible heat flux (latent heat flux) for both day and night. The enhanced hydrological effects, which increase with f_v (Figure 6), result in enhanced reduction in the canopy air temperature (Figure 5) and the wall and ground surface temperatures (Figures 7 and 8). The in-canyon tree canopy dominantly contributes to the hydrological cooling effects compared to the grass/soil surfaces at the canyon floor, and it reduces the wall surface temperature more than the ground surface temperature (not shown). In addition, cooling effects by the tree canopy in the canopy air as well as the surface temperatures tend to increase with h/w, indicating that the physical interaction of the building and tree canopy has a synergic cooling benefit in high-density building areas. A similar effect of in-canyon trees is also found by Ryu *et al.* (2015).

4.3. *Thermodynamic energy balance of the canopy air*

The temporal variation of the canopy air temperature is further examined to quantify the individual contribution of the in-canyon energy-exchanging surfaces (wall, road, grass, soil, and tree) in the in-canyon thermodynamic energy balance. Figure 9 presents diurnal variations of the sensible heat fluxes at the in-canyon surfaces and the canyon top and the canopy air temperature in the base simulation. On the studied summer day, the canopy air temperature begins to increase from 0600 LST, peaks around 1300 LST, and then gradually decreases. In accordance with the temperature variation, the heating/cooling rates of the canopy air remain positive (heating) during 0600–1300 LST (maximum value of $1.7\,^{\circ}\mathrm{C\,h^{-1}}$) but are negative (cooling) in the afternoon and at night. The nocturnal cooling rate is lower than that in the afternoon by $\sim 1\,^{\circ}\mathrm{C\,h^{-1}}$ (Figure 9(b)). The characteristic pattern of the heating/cooling rates is similar to that in observed 2 m temperature (above rooftop) over the Seoul metropolitan area (Lee and Baik, 2011) except that their magnitudes are higher in the canopy air temperature than the 2 m temperature.

Meanwhile, the characteristic variation in the canopy air temperature is determined by a resultant sensible heat flux of the in-canyon energy-exchanging surfaces and the canyon top following Eq. (4). The sensible heat flux at the wall surface has two peaks at ~1000 and ~1600 LST, while at the road surface it peaks ~1200 LST. The temporal profiles of the simulated sensible heat fluxes at the wall and road surfaces are similar to those of the wall and road surface temperatures (e.g. Ryu *et al.*, 2011; Giovannini *et al.*, 2013). The sensible heat fluxes from the wall and road surfaces predominantly contribute to heating

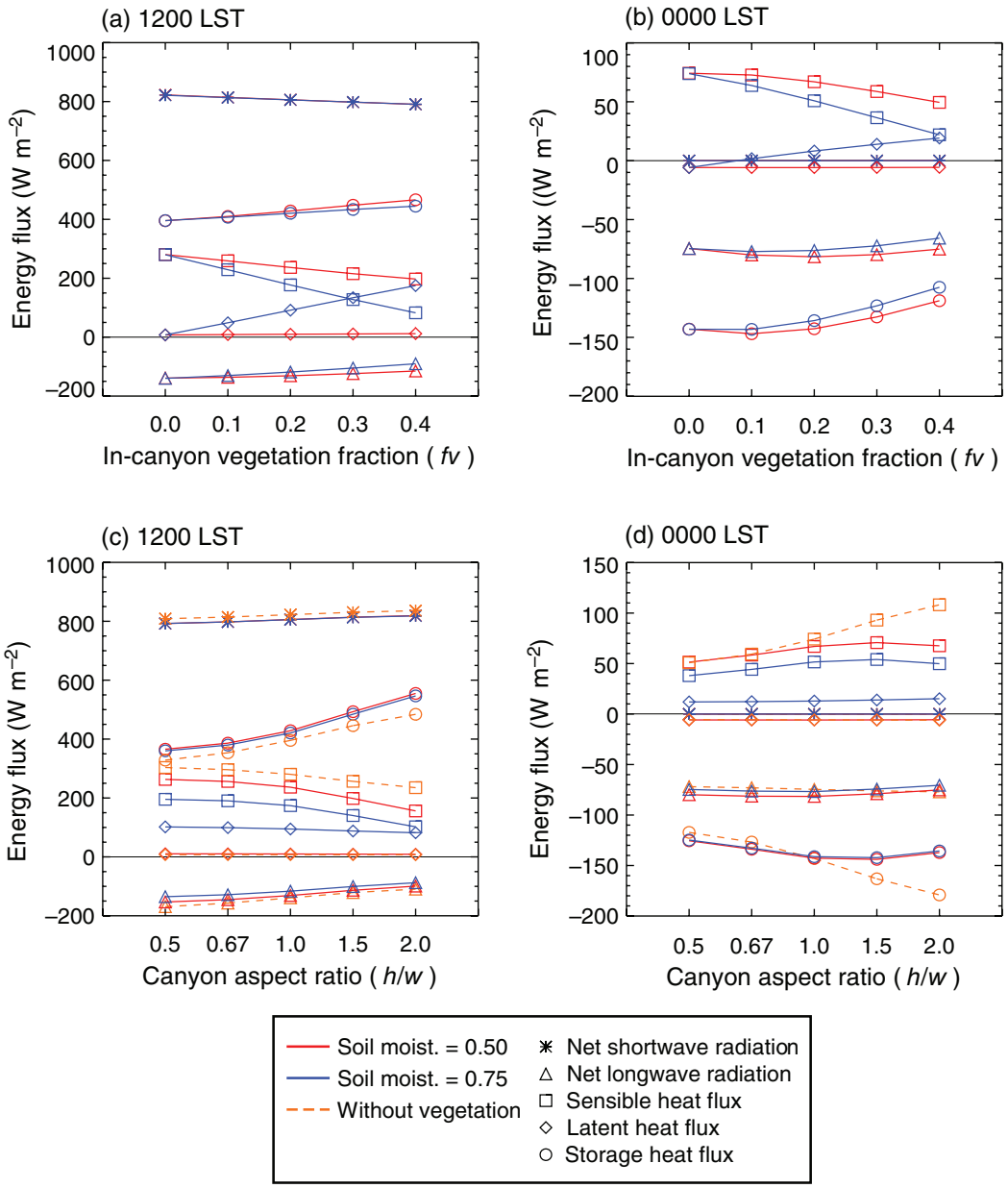

Figure 6. Surface energy balance fluxes at the canyon top at (a, c) noon (1200 LST) and (b, d) midnight (0000 LST) in the simulations versus (a, b) the in-canyon vegetation fraction and (c, d) the canyon aspect ratio.

the canopy air during the diurnal cycle, in which the relative contribution of the wall and road surfaces changes during the diurnal cycle. Meanwhile, the in-canyon vegetation (grass, soil, and tree) slightly contribute to heating the canopy air during daytime, but the contribution is very small compared to the artificial surfaces. At night, the artificial surfaces have positive (toward the canyon) sensible heat fluxes, whereas the vegetated surfaces contribute to cooling the canopy air. The resultant nocturnal sensible heat flux of the in-canyon energy-exchanging surfaces leads to the formation of an unstable atmospheric surface layer due to retardation of the nocturnal canopy air cooling (Figure 9(a)).

Figure 10 compares individual contributions of the in-canyon energy-exchanging surfaces to heating/cooling the canopy air during daytime and at night as a function of in-canyon vegetation fraction and canyon aspect ratio. During daytime, the increase in f_v from 0 to 0.4 gradually reduces the total sensible heat flux from the artificial and natural surfaces by 35% and the sensible heat flux at the canyon top by 30%, in which the reduction at the wall and road surfaces is significant by 62 and 55%, respectively. Under the restricted soil moisture condition, the contribution of the in-canyon vegetation gradually increases with f_v, taking 33% of the total sensible heat flux at $f_v = 0.4$. At night, the sensible heat fluxes from the wall and road surfaces are positive (heating of the canopy air), whereas the sensible heat fluxes from the in-canyon vegetation are negative, indicating lower surface temperatures at the grass surface and tree canopy than the canopy air. On the other hand, the increase in h/w from 0.5 to 2 gradually reduces the total sensible heat flux from the artificial and natural surfaces by 44% and the sensible heat flux at the canyon top by 38% during daytime, in which (as in the change of f_v) the reduction at the wall and road surfaces is significant by 53 and 49%, respectively. The contribution of the in-canyon vegetation gradually increases with h/w, taking 20% of the total sensible heat flux at $h/w = 2$. At night, the sensible heat fluxes at the wall and road surfaces are positive, whereas the sensible heat fluxes from the in-canyon vegetation have negative values, similar to the change in f_v. The sensible heat flux variation at the canyon top in the changes of f_v and h/w is well correlated with that in the total sensible heat flux from the in-canyon energy-exchanging surfaces. The nocturnal sensible heat flux at the canyon top tends to increase as h/w increases, but the variation is not monotonic as a consequence of physical interaction between the building and in-canyon vegetation as discussed above. Provided the soil moisture is enough for hydrological processes of in-canyon vegetation, the sensible heat fluxes from the grass/soil surfaces and the tree

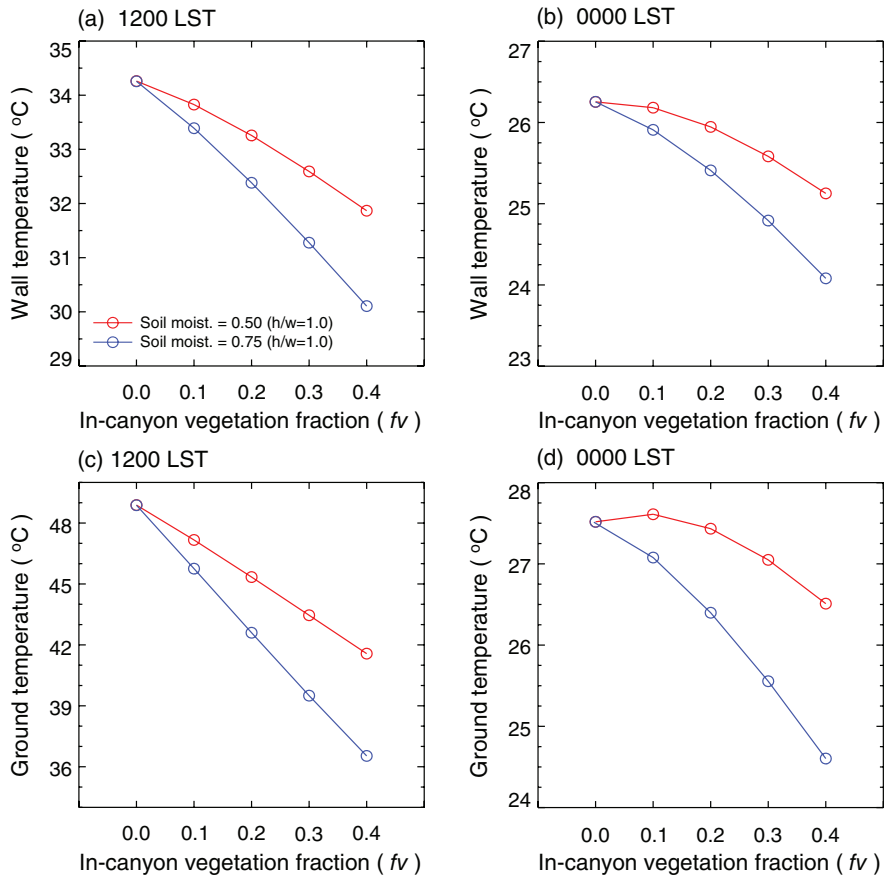

Figure 7. (a, b) Wall and (c, d) ground temperatures at (a, c) noon (1200 LST) and (b, d) midnight (0000 LST) in the simulations changing the in-canyon vegetation fraction. The ground temperature indicates a weight-averaged temperature of the road, grass, and soil surfaces by coverage fraction.

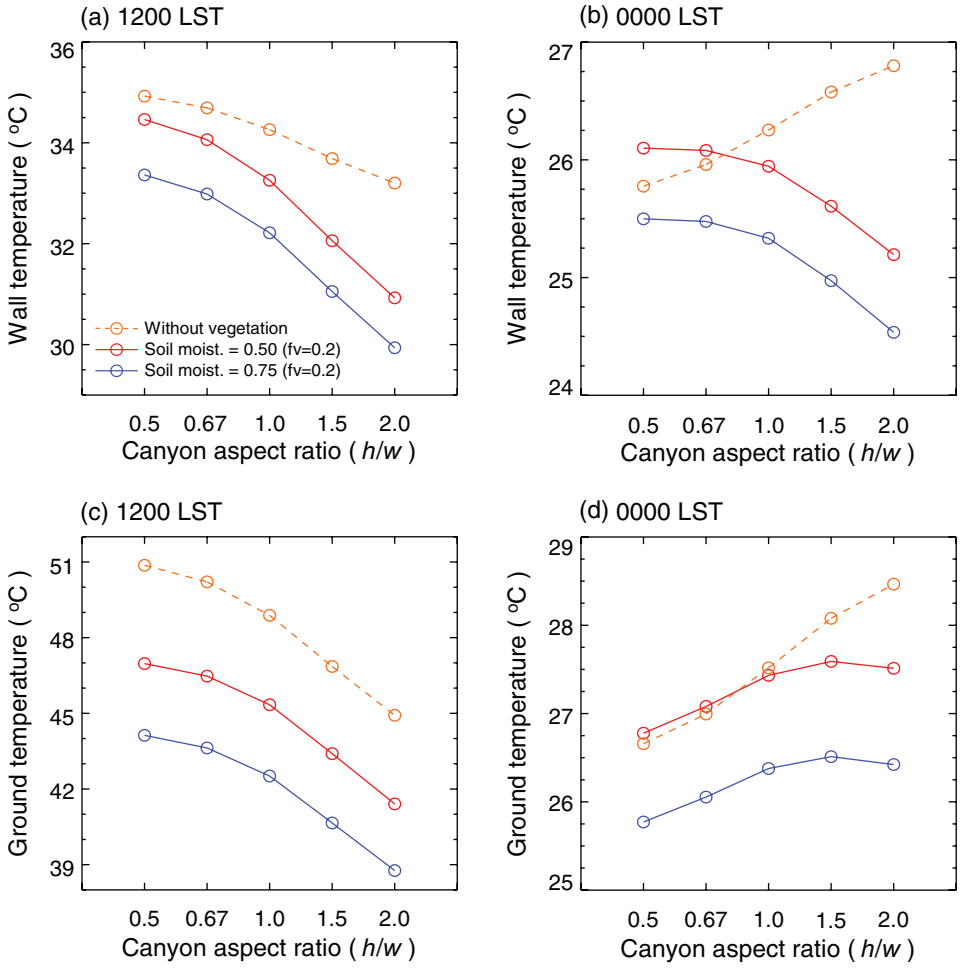

Figure 8. As Figure 7, but for the simulations of the canyon aspect ratio.

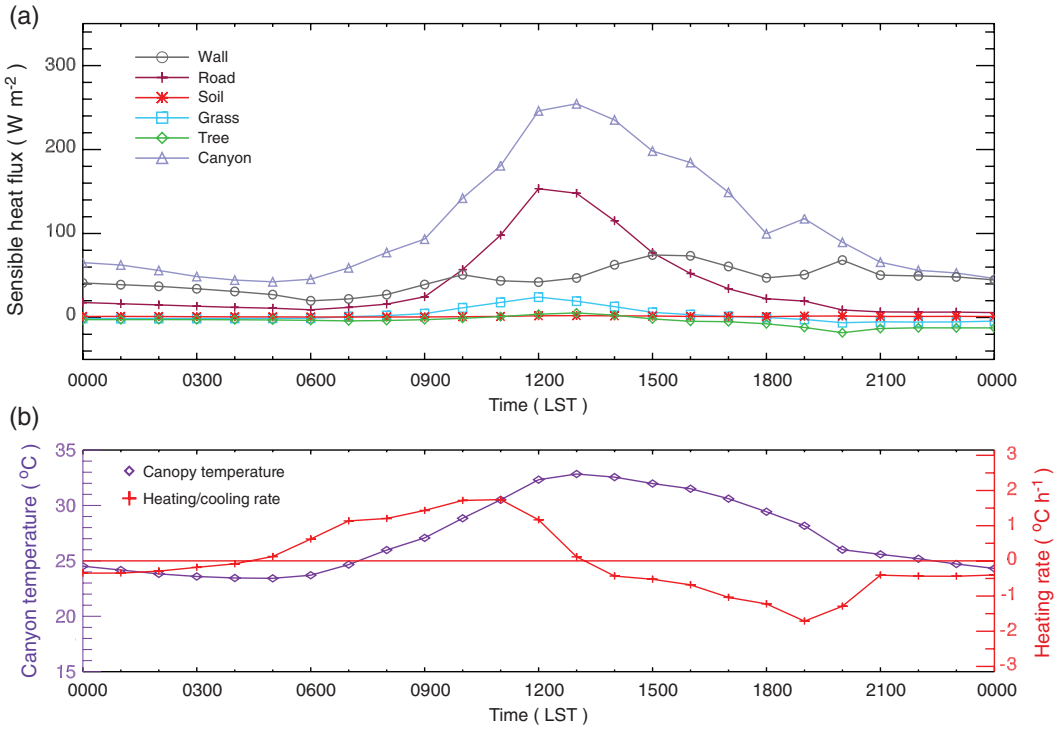

Figure 9. (a) Diurnal variations of the simulated sensible heat fluxes at the wall, road, soil, grass, tree canopy, and the canyon top in the base simulation. The sensible heat flux at each surface is converted to a canyon-equivalent value for comparison. (b) Diurnal variations of the simulated canopy air temperature and heating/cooling rate in the base simulation.

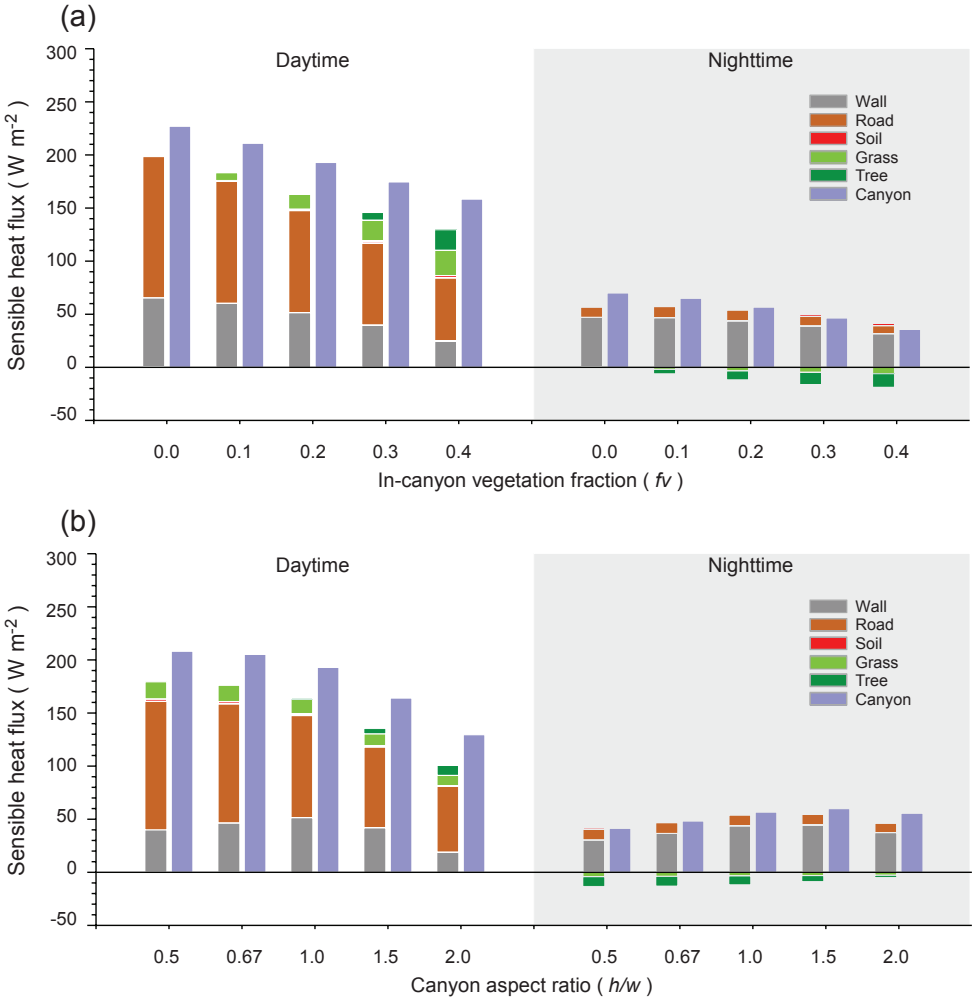

Figure 10. Comparison of the simulated sensible heat fluxes at the wall, road, soil, grass, and tree canopy, and the sensible heat flux at the canyon top for daytime and night-time from the simulations changing (a) the in-canyon vegetation fraction and (b) the canyon aspect ratio. The soil moisture amount is assigned as 50% of the saturation value of sandy clay texture. The sensible heat flux at each surface is converted to a canyon-equivalent value and averaged over 0900–1500 LST for daytime and 2100–0300 LST for night-time.

canopy have negative values (cooling of the canopy air) during daytime and night (not shown), which reduces the sensible heat flux at the canyon top (Figure 6).

5. Summary and conclusions

The VUCM is implemented in the atmospheric model WRF to bridge mesoscale urban modelling to its micrometeorological application in an urban canopy layer. The coupled WRF-VUCM model is capable of explicitly representing building-scale physical processes associated with the artificial and natural surfaces (roof, wall, road, grass, soil, and tree) within an urban street canyon and multi-scale interaction between the canopy air and the overlying atmosphere. The WRF-VUCM simulations are performed for a hot summer day with a fine-grid resolution of 0.333 km and the model's performance in predicting near-surface air temperature is validated against measurements from the 13 urban sites in Seoul. A series of sensitivity simulations are carried out to investigate the impacts of in-canyon vegetation (grass/soil surfaces and trees) and canyon aspect ratio on the thermal environment of street canyons over the Seoul metropolitan area.

The sensitivity simulations show that the existence of in-canyon vegetation decreases the canopy air temperature as well as the wall and ground temperatures during the diurnal cycle. The in-canyon cooling effects increase with in-canyon vegetation fraction even when evapotranspiration is significantly suppressed. In the limited hydrological condition, the radiative and dynamic effects by the in-canyon (tall) tree canopy (relatively to the building height) dominantly contribute to cooling the canopy air compared to the grass/soil surfaces. The in-canyon vegetation's evapotranspiration ('hydrological effects') activated by the increased soil moisture amount is a more efficient pathway to cooling the canopy air and the wall and ground surfaces than its radiative/dynamic effects, which lead also to reduction (increase) of the sensible heat flux (latent heat flux) at the canyon top. On the other hand, a larger canyon aspect ratio (that is, a higher building density) has a cooling effect in the canopy air temperature as well as the wall and ground surfaces during daytime due to the increase in the wall surface area and the shade effect, whereas it has a heating effect due to enhanced trapping of long-wave radiation, which is also found in previous studies (e.g. Marciotto *et al.*, 2010; Ryu *et al.*, 2011; Loughner *et al.*, 2012; Theeuwes *et al.*, 2014). This study shows that the impacts of changing the canyon aspect ratio can be synergistically modulated by the existence of in-canyon vegetation, especially the tree canopy. When the canyon aspect ratio increases above 1, physical interaction between the building and the tree canopy is enhanced, leading to more efficient cooling effects in the canopy air as well as at the wall and ground surfaces. In addition, the hydrological effect by the in-canyon vegetation is also an important factor in enhancing the cooling of the canopy air in the simulations changing the canyon aspect ratio.

In this study, the modelling capability of the coupled WRF-VUCM model is extended to use in a micrometeorological application of the urban canopy layer at the city scale. The simulation results demonstrate the important role of in-canyon vegetation and building density (via canyon aspect ratio) and their nonlinear interaction in simulating the thermal environment of urban street canyons, showing the necessity of physically integrating the parametrization of the building and in-canyon vegetation. In this context, more realistic representation of the urban morphological features using building morphology and infrastructure data in the coupled WRF-VUCM model will be beneficial to accurate simulations of the spatio-temporal variability in the thermal environment of urban street canyons.

Acknowledgements

The authors are grateful to three reviewers and the editor for their useful comments which helped to improve the article. The authors also thank the Korea Meteorological Administration for support with supercomputing resources. This work was supported by the National Research Foundation of Korea (NRF) grant funded by the Korea Ministry of Science, ICT and Future Planning (MSIP) (No. 2011-0017041).

Appendix A: Description of the VUCM model

A: Representation of buildings and in-canyon vegetation

Generally urban surfaces consist of many buildings, permeable surfaces, and trees, which are simply represented in VUCM by a combined framework of the single canyon (Oke, 1988) and the single tree canopy (Lee and Park, 2008; Lee, 2011). The single canyon is composed of the roof, wall, and ground (canyon) surfaces, which is characterized by the mean roof width/fraction (R/f_R), the mean canyon depth (or building height) (H_{building}), and the mean canyon width/fraction (W/f_C), where $f_R + f_C = 1$. The ground surface is composed of the road surface fraction (f_r) and the vegetated grass/soil surfaces fraction (f_v), where $f_r + f_v = 1$. Subsequently, the vegetated surface consists of the grass-covered surface fraction (f_{grs}) and the soil surface fraction (f_s), where $f_{\text{grs}} + f_s = 1$. Meanwhile, the urban trees within the canyon are characterized in the single tree canopy framework by the planar tree fraction within the canyon (f_{tree}), the mean tree height (H_{tree}), and the mean leaf area index (LAI_{tree}) with its density profile (Figure 1). The normalized energy-exchanging surface area of the single tree canopy to the canyon width is defined by $\sigma_l = f_{\text{tree}} LAI^*_{\text{tree}}$, where σ_l is the leaf aspect ratio and LAI^*_{tree} is the effective leaf area index of tree canopy (Lee and Park, 2008). Here, σ_l is introduced to keep an energy conservation law in radiative and turbulent energy exchanges within the canyon. Similarly, $\frac{2h}{w}$ is adopted for the wall surface (Masson, 2000), assuming that two facing walls are identical in terms of the energy exchanges. Based on the six characteristic energy-exchanging surfaces (roof, wall, road, grass, soil, and tree canopy), urban physical processes are parametrized in an interactive way with the canopy air.

B: View factors and transmissivities

Several view factors are required to partition the diffuse radiative energy into urban surfaces, which come from incident diffuse short-wave radiation from the atmosphere, reflected short-wave radiation at the canyon surfaces, and the emitted long-wave radiation from the in-canyon surfaces and urban trees. The wall-sky and ground-sky view factors are defined at the centre of the surfaces by (Swaid, 1993; Masson, 2000)

$$\psi_{wa} = \frac{\frac{1}{2}\left\{\frac{h}{w} + 1 - \left[\left(\frac{h}{w}\right)^2 + 1\right]^{1/2}\right\}}{\frac{h}{w}}, \tag{B1a}$$

$$\psi_{ga} = \left[\left(\frac{h}{w}\right)^2 + 1\right]^{1/2} - \frac{h}{w}, \tag{B1b}$$

where $\frac{h}{w}$ is the canyon aspect ratio. The wall-ground view factor (ψ_{wg}) is identical to ψ_{wa} based on morphological symmetry, while the wall-wall view factor (ψ_{ww}) and the ground-wall view factor (ψ_{gw}) are deduced as $1 - 2\psi_{wa}$ and $1 - \psi_{ga}$, respectively, keeping the energy conservation relation. By symmetry, the sky-ground view factor (ψ_{ag}) and the sky-wall view factor (ψ_{aw}) are also identical to ψ_{ga} and ψ_{gw}, respectively. The tree-sky view factor ($\psi_{l\uparrow}$) and the tree-ground view factor ($\psi_{l\downarrow}$) at the tree canopy are defined in a similar way in ψ_{ga} as

$$\psi_{l\uparrow} = \left[\left(\frac{h - h_{LAD\max}}{w}\right)^2 + 1\right]^{1/2} - \frac{h - h_{LAD\max}}{w}, \tag{B2a}$$

$$\psi_{l\downarrow} = \left[\left(\frac{h_{LAD\max}}{w}\right)^2 + 1\right]^{1/2} - \frac{h_{LAD\max}}{w}, \tag{B2b}$$

where $h_{LAD\max}$ is the height of the tree canopy with a maximum leaf area density. The tree-wall view factor of the tree canopy (ψ_{lw}) is deduced as $2 - \psi_{l\uparrow} - \psi_{l\downarrow}$ for the energy conservation relation.

On the other hand, the transmissivity function of short-wave/long-wave radiation passing through the tree canopy is introduced to compute radiative energy budgets at the in-canyon energy-exchanging surfaces as (Yamada, 1982; Lee and Park, 2008):

$$T(z_1, z_2) = \exp\left(-k\int_{z_1}^{z_2} a\,(z)\,\mathrm{d}z\right), \tag{B3}$$

where $a(z)$ is the leaf area density profile ($\mathrm{m}^2\,\mathrm{m}^{-3}$) of the tree canopy with $\int_0^{h_f} a(z)\mathrm{d}z = LAI_{tree}$ and k is the modulation factor of the tree canopy absorptivity. Here, k is assigned by 0.4 for short-wave radiation, and 0.45 for long-wave radiation. Using the transmissivity function, the radiative transmissivities of the tree canopy are defined as:

$$\tau_{wa} = \tau_{aw} = 1 - f_{tree}\left[1 - T\left(\frac{3}{4}h_b, h_f\right)\right], \tag{B4a}$$

$$\tau_{ww} = 1 - f_{tree}\left[1 - T\left(\frac{1}{4}h_b, \frac{3}{4}h_f\right)\right], \tag{B4b}$$

$$\tau_{wg} = \tau_{gw} = 1 - f_{tree}\left[1 - T\left(0, \frac{1}{4}h_f\right)\right], \tag{B4c}$$

$$\tau_{ga} = \tau_{ag} = 1 - f_{tree}[1 - T(0, h_f)], \tag{B4d}$$

where h_b and h_f are the mean building height and the mean tree height, respectively. The subscripts to τ indicate the start/end points in a radiation transfer path.

C: Short-wave radiation budget

The direct short-wave radiation that reaches at the tree (leaf) canopy (S_l^{D*}) is calculated by

$$S_l^{D*} = S^{D\downarrow} f_{tree}\left\{\frac{2}{\pi}\left[1 - T\left(h_c, h_f\right)\right] + \left(1 - \frac{2}{\pi}\right)[1 - T(0, h_f)]\right\}, \tag{C1}$$

where $S^{D\downarrow}$ is the downward direct short-wave radiative flux incident into the canyon and h_c is the shaded height of the tree canopy by the building (Figure 3 in Lee and Park, 2008). Here, the interior canyon angle (θ_n) between the canyon axis and the solar azimuth angle (Lee and Park, 2008) is averaged in direction, leading to $\frac{2}{\pi}$. The shaded height of the tree canopy is calculated by $h_c = h_b - w/(2\tan\theta_z \sin\theta_n)$, where θ_z is the solar zenith angle. The shading effects by the tree canopy as well as the building are considered in the in-canyon direct solar radiation transfer. The direct solar radiation absorbed by the tree canopy is calculated as

$$S_l^{D\downarrow} = S_l^{D*}(1 - \alpha_l)/\sigma_l. \tag{C2}$$

On the other hand, the direct short-wave radiation that reaches the wall, ground (canyon floor), road, and grass/soil surfaces is

$$S_w^{D\downarrow} = (S^{D\downarrow} - S_l^{D*\downarrow}) \begin{cases} \frac{1}{\pi}\frac{w}{h} & \text{if } \theta_z \geq \arctan\left(\frac{w}{h}\right) \\ \frac{1}{\pi}\tan\theta_z & \text{if } \theta_z < \arctan\left(\frac{w}{h}\right) \end{cases}, \tag{C3a}$$

$$S_g^{D\downarrow} = (S^{D\downarrow} - S_l^{D*\downarrow}) \begin{cases} 1 - \frac{2}{\pi} & \text{if } \theta_z \geq \arctan\left(\frac{w}{h}\right) \\ 1 - \frac{2}{\pi}\frac{h}{w}\tan\theta_z & \text{if } \theta_z < \arctan\left(\frac{w}{h}\right) \end{cases}, \tag{C3b}$$

$$S_r^{D\downarrow} = f_r S_g^{D\downarrow}, \tag{C3c}$$

$$S_{grs}^{D\downarrow} = f_v f_{grs} S_g^{D\downarrow}, \tag{C3d}$$

$$S_s^{D\downarrow} = f_v f_s S_g^{D\downarrow}. \tag{C3e}$$

Here, the interior canyon angle (θ_n) is averaged in direction. The incident radiation is first partitioned into the wall and ground surfaces, and then the radiation reaching the ground surface is re-partitioned into the road and grass/soil surfaces. In addition, the shading effect by the tree canopy influences all the other in-canyon energy-exchanging surfaces.

The diffuse short-wave radiation that reaches at the tree canopy (S_l^{I*}) is calculated from

$$S_l^{I*} = S^{I\downarrow} f_{tree}[1 - T(0, h_f)] = S^{I\downarrow}(1 - \tau_{ag}), \tag{C4}$$

where $S^{I\downarrow}$ is the downward diffuse short-wave radiative flux incident at the canyon top. The absorbed diffuse solar radiation by the tree canopy is calculated as

$$S_l^{I\downarrow} = S_l^{I*}(1 - \alpha_l)(1 - \psi_{l\uparrow})/\sigma_l. \tag{C5}$$

The diffuse short-wave radiation that reaches the wall, ground, road, and grass/soil surfaces is

$$S_w^{I\downarrow} = (S^{I\downarrow} - S_l^{I*\downarrow})\psi_{aw}, \tag{C6a}$$

$$S_g^{I\downarrow} = (S^{I\downarrow} - S_l^{I*\downarrow})\psi_{ag}, \tag{C6b}$$

$$S_r^{I\downarrow} = f_r S_g^{I\downarrow}, \tag{C6c}$$

$$S_{grs}^{I\downarrow} = f_v f_{grs} S_g^{I\downarrow}, \tag{C6d}$$

$$S_s^{I\downarrow} = f_v f_s S_g^{I\downarrow}. \tag{C6e}$$

The radiative trapping effect in short-wave radiation is represented by three times reflection of the incident direct/diffuse radiation at each surface. After the final reflection, the radiative energy reaching a surface is assumed to be totally absorbed at the surface to satisfy the energy conservation. The net short-wave radiation at the wall, ground, road, grass/soil surfaces, and the tree canopy is calculated as

$$S_w^{\downarrow\uparrow} = (S_w^{D\downarrow} + S_w^{I\downarrow}) \begin{bmatrix} (1-\alpha_w) + \tau_{wg}\tau_{gw}\alpha_w\overline{\alpha}_g\psi_{wg} \\ \psi_{gw}(1-\alpha_w) + \tau_{ww}\tau_{wg}\tau_{gw}\alpha_w^2 \\ \overline{\alpha}_g\psi_{ww}\psi_{wg}\psi_{gw} + \tau_{ww}\alpha_w\psi_{ww}(1-\alpha_w) \\ +\tau_{ww}^2\alpha_w^2\psi_{ww}^2(1-\alpha_w) + \tau_{ww}^3\alpha_w^3\psi_{ww}^3 \end{bmatrix}$$
$$+(S_g^{D\downarrow} + S_g^{I\downarrow}) \begin{bmatrix} \tau_{gw}\overline{\alpha}_g\psi_{gw}\,(1-\alpha_w) + \tau_{gw}\tau_{ww}\overline{\alpha}_g \\ \alpha_w\psi_{gw}\psi_{ww}(1-\alpha_w) + \tau_{gw}\tau_{ww}^2 \\ \overline{\alpha}_g\alpha_w^2\psi_{gw}\psi_{ww}^2 + \tau_{gw}^2\tau_{wg}\overline{\alpha}_g^2\alpha_w\psi_{gw}^2\psi_{wg} \end{bmatrix}, \tag{C7a}$$

$$S_g^{\downarrow\uparrow} = (S_w^{D\downarrow} + S_w^{I\downarrow}) \begin{bmatrix} \tau_{wg}\alpha_w\psi_{wg}\left(1-\overline{\alpha}_g\right) + \tau_{ww}^2\tau_{wg}\alpha_w^2\overline{\alpha}_g\psi_{ww}^2\psi_{wg} \\ +\tau_{ww}^2\alpha_w^2\psi_{ww}^2\psi_{wg}(1-\overline{\alpha}_g) + \tau_{ww}^3\alpha_w^3\psi_{ww}^3\psi_{wg} \end{bmatrix} + (S_g^{D\downarrow} + S_g^{I\downarrow}) \begin{bmatrix} \left(1-\overline{\alpha}_g\right) + \tau_{gw}\tau_{wg}\overline{\alpha}_g\alpha_w\psi_{gw}\psi_{wg}(1-\overline{\alpha}_g) \\ +\tau_{gw}\tau_{ww}^2\overline{\alpha}_g\alpha_w^2\psi_{gw}\psi_{ww}^2\psi_{wg} \end{bmatrix}, \tag{C7b}$$

$$S_r^{\downarrow\uparrow} = f_r(1-\alpha_r)S_g^{\downarrow\uparrow}/(1-\overline{\alpha}_g), \tag{C7c}$$

$$S_{grs}^{\downarrow\uparrow} = f_v f_{grs}(1-\alpha_{grs})S_g^{\downarrow\uparrow}/(1-\overline{\alpha}_g), \tag{C7d}$$

$$S_s^{\downarrow\uparrow} = f_v f_s(1-\alpha_s)S_g^{\downarrow\uparrow}/(1-\overline{\alpha}_g), \tag{C7e}$$

$$S_l^{\downarrow\uparrow} = \frac{\begin{bmatrix} \sigma_l\left(S_l^{D\downarrow} + S_l^{I\downarrow}\right) + \frac{2h}{w}(S_w^{D\downarrow} + S_w^{I\downarrow}) \\ +(S_g^{D\downarrow} + S_g^{I\downarrow}) - \frac{2h}{w}S_w^{\downarrow\uparrow} - S_g^{\downarrow\uparrow} - S_{atm}^{\uparrow} \end{bmatrix}}{\sigma_l}, \tag{C7f}$$

where $\overline{\alpha}_g$ is a weight-averaged albedo of the road and grass/soil surfaces and $S_{atm}^{\uparrow}$ is the short-wave radiation back into the atmosphere. In the radiative transfer process, the net short-wave radiation of the wall and ground surfaces are first calculated using the view factors and the transmissivities of the tree canopy, and then the net radiation of the road and grass/soil surfaces are calculated from the net radiation of the ground surface. The net radiation at the tree canopy is calculated by using the energy conservation relation for simplicity.

D: Long-wave radiation budget

The tree canopy is a source of long-wave radiation within the canyon, and the radiation emitted from the tree canopy is distributed to the tree canopy itself (tree-tree exchange) as well as the wall, road, and grass/soil surfaces. The long-wave radiation from the tree canopy is assumed to be isotropically emitted at the height of $h_{LAD\,\max}$, and the radiative energy reaching each surface is totally absorbed at the surface without reflection. The long-wave radiation emitted from the tree canopy is partitioned to the tree canopy, wall, ground, road, grass/soil surfaces, and the atmosphere as:

$$L_l^{l\uparrow} = L^{l\uparrow}f_{tree}[1 - T(0,h_f)] = L^{l\uparrow}(1-\tau_{ga}), \tag{D1a}$$

$$L_w^{l\uparrow} = 0.5\sigma_l[L^{l\uparrow} - L_l^{l\uparrow}](2 - \psi_{l\uparrow} - \psi_{l\downarrow})\frac{w}{2h}, \tag{D1b}$$

$$L_g^{l\uparrow} = 0.5\sigma_l[L^{l\uparrow} - L_l^{l\uparrow}]\psi_{l\downarrow}, \tag{D1c}$$

$$L_r^{l\uparrow} = f_r L_g^{l\uparrow}, \tag{D1d}$$

$$L_{grs}^{l\uparrow} = f_v f_{grs} L_g^{l\uparrow}, \tag{D1e}$$

$$L_s^{l\uparrow} = f_v f_s L_g^{l\uparrow}, \tag{D1f}$$

$$L_a^{l\uparrow} = 0.5\sigma_l[L^{l\uparrow} - L_l^{l\uparrow}]\psi_{l\uparrow}, \tag{D1g}$$

where the long-wave radiation from the tree canopy is given by $L^{l\uparrow} = \sigma_l\varepsilon_l\sigma T_l^4$.

The radiative trapping effect in long-wave radiation transfer is represented by one reflection at each surface within the canyon due to large emissivity (absorptivity) of the in-canyon surfaces. Similarly, in the short-wave radiation, the radiative energy reaching a surface after reflection is assumed to be totally absorbed at the same surface to ensure energy conservation. The net long-wave radiation at the wall, ground, road, grass/soil surfaces, and the tree canopy are calculated by

$$\begin{aligned} L_w^{\downarrow\uparrow} &= \tau_{aw}\varepsilon_w\psi_{aw}L^{atm\downarrow} + \tau_{ww}\varepsilon_w\psi_{ww}L^{w\uparrow} + \tau_{gw}\varepsilon_w\psi_{gw}\overline{L}^{g\uparrow} \\ &+\tau_{ag}\tau_{gw}(1-\overline{\varepsilon}_g)\psi_{ag}\psi_{gw}L^{atm\downarrow} + \tau_{aw}\tau_{ww}(1-\varepsilon_w)\psi_{aw}\psi_{ww}L^{atm\downarrow} \\ &+\tau_{wg}\tau_{gw}(1-\overline{\varepsilon}_g)\psi_{wg}\psi_{gw}L^{w\uparrow} + \tau_{ww}^2(1-\varepsilon_w)\psi_{ww}^2L^{w\uparrow} \\ &+\tau_{gw}\tau_{ww}(1-\varepsilon_w)\psi_{gw}\psi_{ww}\overline{L}^{g\uparrow} + L_{l\uparrow}^{w} - L^{w\uparrow}, \end{aligned} \tag{D2a}$$

$$\begin{aligned} L_g^{\downarrow\uparrow} &= \tau_{ag}\overline{\varepsilon}_g\psi_{ag}L^{atm\downarrow} + \tau_{wg}\overline{\varepsilon}_g\psi_{wg}L^{w\uparrow} \\ &+\tau_{aw}\tau_{wg}(1-\varepsilon_w)\psi_{aw}\psi_{wg}L^{atm\downarrow} + \tau_{ww}\tau_{wg}(1-\varepsilon_w)\psi_{ww}\psi_{wg}L^{w\uparrow} \\ &+\tau_{gw}\tau_{wg}(1-\varepsilon_w)\psi_{gw}\psi_{wg}\overline{L}^{g\uparrow} + L_g^{l\uparrow} - L^{g\uparrow}, \end{aligned} \tag{D2b}$$

$$L_r^{\downarrow\uparrow} = f_r\varepsilon_r L_g^{\downarrow\uparrow}/\overline{\varepsilon}_g, \tag{D2c}$$

$$L_{grs}^{\downarrow\uparrow} = f_v f_{grs}\varepsilon_{grs} L_g^{\downarrow\uparrow}/\overline{\varepsilon}_g, \tag{D2d}$$

$$L_s^{\downarrow\uparrow} = f_v f_s\varepsilon_s L_g^{\downarrow\uparrow}/\overline{\varepsilon}_g, \tag{D2e}$$

$$L_l^{\downarrow\uparrow} = \frac{\begin{bmatrix} L^{atm\downarrow} + \frac{2h}{w}L^{w\uparrow} + \overline{L}^{g\uparrow} + \sigma_l L_l^{l\uparrow} - \\ \frac{2h}{w}L_{w\downarrow} - L_{g\downarrow} - L_{atm\uparrow} - \sigma_l L^{l\uparrow} \end{bmatrix}}{\sigma_l}, \tag{D2f}$$

where $\overline{\varepsilon}_g$ is a weight-averaged emissivity of the road and grass/soil surfaces and $L_{atm\uparrow}$ is the long-wave radiation going into the atmosphere.

E: Turbulent fluxes of momentum, heat, and moisture

The turbulent sensible heat and moisture fluxes at the roof surface are calculated based on the Monin-Obukhov similarity theory as (Kot and Song, 1998):

$$\begin{aligned} H_R &= -\rho\, c_p u_{*,R}\theta_{*,R} \\ &= -\rho c_p \frac{k^2 F_h\left(\frac{z-h_b}{z_{0,R}}, \frac{z-h_b}{z_{0T,R}}, Ri_B\right) u^{atm}(\theta^{atm} - \theta_{s,R})}{\left(\ln\frac{z}{z_{0,R}}\ln\frac{z}{z_{0T,R}}\right)}, \end{aligned} \tag{E1a}$$

$$E_R = -\rho u_{*,R}q_{*,R} = -\rho\frac{k^2 F_q\left(\frac{z-h_b}{z_{0,R}}, \frac{z-h_b}{z_{0q,R}}, Ri_B\right) u^{atm}(q^{atm} - q_{s,R})}{\left(\ln\frac{z-h_b}{z_{0,R}}\ln\frac{z-h_b}{z_{0q,R}}\right)}, \tag{E1b}$$

where u_*, θ_*, q_* are the friction velocity, the temperature characteristic scale, and the moisture characteristic scale of the atmospheric surface layer, k is the von Kármán constant, F represents the stability correction function, z_0 and z_{0T} are the roughness lengths for momentum and heat, Ri_B is the Bulk Richardson number defined by $Ri_B = \frac{gz\Delta\theta}{\theta u^{atm}}\frac{(1-z_0/z)^2}{(1-z_{0T}/z)}$, h_b is the mean building height, and the subscript R stands for the roof surface. Similarly, the turbulent exchanges of the sensible heat and

moisture between the canopy air and the overlying atmosphere are calculated as

$$H_C = -\rho c_p u_{*,C}\theta_{*,C} = \rho c_p \frac{k^2 F_h\left(\frac{z-d}{z_0}, \frac{z-d}{z_{0T}}, Ri_B\right) u^{atm}(\theta^{atm} - \theta_C)}{\left(\ln\frac{z-d}{z_0}\ln\frac{z-d}{z_{0T}}\right)}, \tag{E2a}$$

$$E_C = -\rho u_{*,C} q_{*,C} = -\rho \frac{k^2 F_q\left(\frac{z-d}{z_0}, \frac{z-d}{z_{0q}}, Ri_B\right) u^{atm}(q^{atm} - q_C)}{\left(\ln\frac{z-d}{z_0}\ln\frac{z-d}{z_{0q}}\right)}, \tag{E2b}$$

The turbulent heat and moisture fluxes calculated at the roof surface and the canyon are weight-averaged for the turbulent fluxes of an urban patch. Meanwhile, the turbulent momentum flux of the urban patch is calculated as:

$$\tau = -\rho\, u_* u_* = -\rho \frac{k^2 F_m\left(\frac{z-d}{z_0}, Ri_B\right) u^{atm2}}{\left(\ln\frac{z-d}{z_0}\right)^2}, \tag{E3}$$

On the other hand, the turbulent heat and moisture exchanges within the urban canopy layer occur between the in-canyon energy-exchanging surfaces (wall, road, grass/soil, tree canopy) and the canopy air. The turbulent sensible heat exchange between the wall surface and the canopy air is parametrized using an empirical Jurges' formula (Rowley *et al.*, 1930), and the turbulent heat and moisture exchanges between the road surface and the canopy air are calculated with the same similarity relations used for the roof surface using the reference height of the zero-plane displacement height (d) and the roughness lengths for momentum and heat ($z_{0,r}$ and $z_{0T,r}$) for the road surface. The turbulent heat and moisture exchanges between the in-canyon vegetation (grass/soil, tree canopy) and the canopy air are calculated based on the resistance formulations (e.g. Avissar and Pielke, 1989). More detailed formulations can be found in Lee and Park (2008) and Lee (2011).

References

Alexandri E, Jones P. 2008. Temperature decreases in an urban canyon due to green walls and green roofs in diverse climates. *Build. Environ.* **43**: 480–493, doi: 10.1016/j.buildenv.2006.10.055.

Ali-Toudert F, Mayer H. 2006. Numerical study on the effects of aspect ratio and orientation of an urban street canyon on outdoor thermal comfort in hot and dry climate. *Build. Environ.* **41**: 94–108, doi: 10.1016/j.buildenv.2005.01.013.

Avissar R, Pielke RA. 1989. A parameterization of heterogeneous land surface for atmospheric numerical models and its impact on regional meteorology. *Mon. Weather Rev.* **117**: 2113–2136, doi: 10.1175/1520-0493(1989)117<2113:APOHLS>2.0.CO;2.

Best MB, Grimmond CSB. 2014. Importance of initial state and atmospheric conditions for urban land surface models' performance. *Urban Clim.* **10**: 387–406, doi: 10.1016/j.uclim.2013.10.006.

Best MB, Grimmond CSB. 2015. Key conclusions of the first international urban land surface model comparison project. *Bull. Am. Meteorol. Soc.* **96**: 805–819, doi: 10.1175/BAMS-D-14-00122.1.

Chen F, Dudhia J. 2001. Coupling an advanced land-surface-hydrology model with the Penn State-NCAR MM5 modeling system. Part I: Model description and implementation. *Mon. Weather Rev.* **129**: 569–585, doi: 10.1175/1520-0493(2001)129<0569:CAALSH>2.0.CO;2.

Chen F, Kusaka H, Bornstein R, Ching J, Grimmond CSB, Grossman-Clarke S, Loridan T, Manning KW, Martilli A, Miao S, Sailor D, Salamanca FP, Taha H, Tewari M, Wang X, Wyszogrodzki AA, Zhang C. 2011. The integrated WRF/urban modelling system: Development, evaluation, and applications to urban environmental problems. *Int. J. Climatol.* **31**: 273–288, doi: 10.1002/joc.2158.

Dimoudi A, Kantzioura A, Zoras S, Pallas C, Kosmopoulos P. 2013. Investigation of urban microclimate parameters in an urban center. *Energy Build.* **64**: 1–9, doi: 10.1016/j.enbuild.2013.04.014.

Dudhia J. 1989. Numerical study of convection observed during the winter monsoon experiment using a mesoscale two-dimensional model. *J. Atmos. Sci.* **46**: 3077–3107, doi: 10.1175/1520-0469(1989)046<3077:NSOCOD>2.0.CO;2.

Dupont S, Mestayer PG. 2006. Parameterization of the urban energy budget with the submesoscale soil model. *J. Appl. Meteorol. Climatol.* **45**: 1744–1765, doi: 10.1175/JAM2417.1.

Giovannini L, Zardi D, De Franceschi M. 2013. Characterization of the thermal structure inside an urban canyon: Field measurement and validation of a simple model. *J. Appl. Meteorol. Climatol.* **52**: 64–81, doi: 10.1175/JAMC-D-12-06.1.

Giridharan R, Lau SSY, Ganesan S, Givoni B. 2008. Lowering the outdoor temperature in high-rise high-density residential developments of coastal Hong Kong: The vegetation influence. *Build. Environ.* **43**: 1583–1595, doi: 10.1016/j.buildenv.2007.10.003.

Grimm NB, Foster D, Groffman P, Grove J, Hopkinson C, Nadelhoffer K, Pataki D, Peters D. 2008. The changing landscape: Ecosystem responses to urbanization and pollution across climatic and societal gradients. *Front. Ecol. Environ.* **6**: 264–272, doi: 10.1890/070147.

Grimmond CSB, Blackett M, Best MJ, Barlow J, Baik J-J, Belcher SE, Bohnenstengel SI, Calmet I, Chen F, Dandou A, Fortuniak K, Gouvea ML, Hamdi R, Hendry M, Kawai T, Kawamoto Y, Kondo H, Krayenhoff ES, Lee S-H, Loridan T, Martilli A, Masson V, Miao S, Oleson K, Pigeon G, Porson A, Ryu Y-H, Salamanca F, Shashua-Bar L, Steeneveld G-J, Tombrou M, Voogt J, Young D, Zhang N. 2010. The international urban energy balance models comparison project: First results from phase 1. *J. Appl. Meteorol. Climatol.* **49**: 1268–1292, doi: 10.1175/2010JAMC2354.1.

Grimmond CSB, Blackett M, Best MJ, Baik J-J, Belcher SE, Beringer J, Bohnenstengel SI, Calmet I, Chen F, Coutts A, Dandou A, Fortuniak K, Gouvea ML, Hamdi R, Hendry M, Kanda M, Kawai T, Kawamoto Y, Kondo H, Krayenhoff ES, Lee S-H, Loridan T, Martilli A, Masson V, Miao S, Oleson K, Ooka R, Pigeon G, Porson A, Ryu Y-H, Salamanca F, Steeneveld G-J, Tombrou M, Voogt JA, Young DT, Zhang N. 2011. Initial results from phase 2 of the international urban energy balance model comparison. *Int. J. Climatol.* **31**: 244–272, doi: 10.1002/joc.2227.

Högström U. 1996. Review of some basic characteristics of the atmospheric surface layer. *Boundary-Layer Meteorol.* **78**: 215–246, doi: 10.1007/BF00120937.

Hong S-Y, Lim J-OJ. 2006. The WRF single-moment 6-class microphysics scheme (WSM6). *J. Korean Meteorol. Soc.* **42**: 129–151.

Hong S-Y, Noh Y, Dudhia J. 2006. A new vertical diffusion package with an explicit treatment of entrainment processes. *Mon. Weather Rev.* **134**: 2318–2341, doi: 10.1175/MWR3199.1.

Jimenez PA, Dudhia J, Gonzalez-Rouco JF, Navarro J, Montavez JP, Garcia-Bustamante E. 2012. A revised scheme for the WRF surface layer formulation. *Mon. Weather Rev.* **140**: 898–918, doi: 10.1175/MWR-D-11-00056.1.

Kain JS. 2004. The Kain-Fritsch convective parameterization: An update. *J. Appl. Meteorol.* **43**: 170–181, doi: 10.1175/1520-0450(2004)043<0170:TKCPAU>2.0.CO;2.

Kim Y-H, Baik J-J. 2005. Spatial and temporal structure of the urban heat island in Seoul. *J. Appl. Meteorol.* **44**: 591–605, doi: 10.1175/JAM2226.1.

Kot SC, Song Y. 1998. An improvement of the Louis scheme for the surface layer in an atmospheric modelling system. *Boundary-Layer Meteorol.* **88**: 239–254.

Krayenhoff ES, Voogt JA. 2010. Impacts of urban albedo increase on local air temperature at daily-annual time scales: Model results and synthesis of previous work. *J. Appl. Meteorol. Climatol.* **49**: 1634–1648, doi: 10.1175/2010JAMC2356.1.

Krayenhoff ES, Christen A, Martilli A, Oke TR. 2014. A multi-layer radiation model for urban neighbourhoods with trees. *Boundary-Layer Meteorol.* **151**: 139–178.

Krayenhoff ES, Santiago JL, Martilli A, Christen A, Oke TR. 2015. Parameterization of drag and turbulence for urban neighbourhoods with trees. *Boundary-Layer Meteorol.* **156**: 157–189, doi: 10.1007/s10546-015-0028-6.

Kunkel KE, Changnon SA, Reinke BC, Arritt RW. 1996. The July 1995 heat wave in the Midwest: A climatic perspective and critical weather factors. *Bull. Am. Meteorol. Soc.* **77**: 1507–1518, doi: 10.1175/1520-0477(1996)077<1507:TJHWIT>2.0.CO;2.

Kusaka H, Kondo H, Kikegawa Y, Kimura F. 2001. A simple single-layer urban canopy model for atmospheric models: Comparison with multi-layer and slab models. *Boundary-Layer Meteorol.* **101**: 329–358, doi: 10.1023/A:1019207923078.

Kusaka H, Chen F, Tewari M, Dudhia J, Gill DO, Duda MG, Wang W, Miya Y. 2012. Numerical simulation of urban heat island effect by the WRF model with 4-km grid increment: An intercomparison study between the urban canopy model and slab model. *J. Meteorol. Soc. Jpn.* **90B**: 33–45, doi: 10.2151/jmsj.2012-B03.

Lee S-H. 2011. Further development of the vegetated urban canopy model including a grass-covered surface parameterization and photosynthesis effects. *Boundary-Layer Meteorol.* **140**: 315–342, doi: 10.1007/s10546-011-9603-7.

Lee S-H, Baik J-J. 2011. Evaluation of the Vegetated Urban Canopy Model (VUCM) and its impacts on urban boundary layer simulation. *Asia-Pac. J. Atmos. Sci.* **47**: 151–165, doi: 10.1007/s13143-011-0005-z.

Lee S-H, Kim S-T. 2015. Estimation of anthropogenic heat emission over South Korea using a statistical regression method. *Asia-Pac. J. Atmos. Sci.* **51**: 157–166, doi: 10.1007/s13143-015-0065-6.

Lee S-H, Park S-U. 2008. A vegetated urban canopy model for meteorological and environmental modelling. *Boundary-Layer Meteorol.* **126**: 73–102, doi: 10.1007/s10546-007-9221-6.

Lee S-H, Kim S-W, Angevine WM, Bianco L, McKeen SA, Senff CJ, Zamora RJ. 2011. Evaluation of urban surface parameterizations in the WRF model using measurements during the Texas Air Quality Study 2006 field campaign. *Atmos. Chem. Phys.* **11**: 2127–2143, doi: 10.5194/acp-11-2127-2011.

Lemonsu A, Masson V, Shashua-Bar L, Erel E, Pearlmutter D. 2012. Inclusion of vegetation in the town energy balance model for modelling urban green areas. *Geosci. Model Dev.* **5**: 1377–1393, doi: 10.5194/gmd-5-1377-2012.

Li D, Bou-Zeid E. 2013. Synergistic interactions between urban heat islands and heat waves: The impact in cities is larger than the sum of its parts. *J. Appl. Meteorol. Climatol.* **52**: 2051–2064, doi: 10.1175/JAMC-D-13-02.1.

Li D, Bou-Zeid E. 2014. Quality and sensitivity of high-resolution numerical simulation of urban heat islands. *Environ. Res. Lett.* **9**: 055001, doi: 10.1088/1748-9326/9/5/055001.

Li X, Norford LK. 2016. Evaluation of cool roof and vegetations in mitigating urban heat island in a tropical city, Singapore. *Urban Clim.* **16**: 59–74, doi: 10.1016/j.uclim.2015.12.002.

Loughner CP, Allen DJ, Zhang D-L, Pickering KE, Dickerson RR, Landry L. 2012. Roles of urban tree canopy and buildings in urban heat island effects: Parameterization and preliminary results. *J. Appl. Meteorol. Climatol.* **51**: 1775–1793, doi: 10.1175/JAMC-D-11-0228.1.

Marciotto ER, Oliveira AP, Hanna SR. 2010. Modeling study of the aspect ratio influence on urban canopy energy fluxes with a modified wall-canyon energy budget scheme. *Build. Environ.* **45**: 2497–2505, doi: 10.1016/j.buildenv.2010.05.012.

Martilli A. 2014. An idealized study of city structure, urban climate, energy consumption, and air quality. *Urban Clim.* **10**: 430–446, doi: 10.1016/j.uclim.2014.03.003.

Martilli A, Clappier A, Rotach MW. 2002. An urban surface exchange parameterization for mesoscale models. *Boundary-Layer Meteorol.* **104**: 261–304, doi: 10.1023/A:1016099921195.

Masson V. 2000. A physically-based scheme for the urban energy budget. *Boundary-Layer Meteorol.* **94**: 357–397, doi: 10.1023/A:1002463829265.

Masson V, Marchadier C, Adolphe L, Aguejdad R, Avner P, Bonhomme M, Bretagne G, Briottet X, Bueno B, De Munch C, Doukari O, Hallegatte S, Hidalgo J, Houet T, Le Bras J, Lemonsu A, Long N, Moine M-P, Morel T, Nolorgues L, Pigeon G, Salagnac J-L, Viguie V, Zibouche K. 2014. Adapting cities to climate change: A systemic modelling approach. *Urban Clim.* **10**: 407–429, doi: 10.1016/j.uclim.2014.03.004.

Mlawer EJ, Taubman SJ, Brown PD, Iacono MJ, Clough SA. 1997. Radiative transfer for inhomogeneous atmospheres: RRTM, a validated correlated-*k* model for the longwave. *J. Geophys. Res.* **102**: 16663–16682, doi: 10.1029/97JD00237.

Montgomery MR. 2008. The urban transformation of the developing world. *Science* **319**: 761–764, doi: 10.1126/science.1153012.

Ng E, Chen L, Wang Y, Yuan C. 2012. A study on the cooling effects of greening in a high-density city: An experience from Hong Kong. *Build. Environ.* **47**: 256–271, doi: 10.1016/j.buildenv.2011.07.014.

Niachou K, Livata I, Santamouris M. 2008. Experimental study of temperature and airflow distribution inside an urban street canyon during hot summer weather conditions. Part I: Air and surface temperatures. *Build. Environ.* **43**: 1383–1392, doi: 10.1016/j.buildenv.2007.01.039.

Oke TR. 1982. The energetic basis of the urban heat island. *Q. J. R. Meteorol. Soc.* **108**: 1–24, doi: 10.1002/qj.49710845502.

Oke TR. 1988. Street design and urban canopy layer climate. *Build. Environ.* **11**: 103–113, doi: 10.1016/0378-7788(88)90026-6.

Oke TR. 2006. 'Initial guidance to obtain representative meteorological observations at urban sites. Instrumentation and observing methods'. Report No. 81. World Meteorological Organization: Geneva, Switzerland.

Oleson KW, Bonan GB, Feddema J, Vertenstein M, Grimmond CSB. 2008. An urban parameterization for a global climate model. Part I: Formulation and evaluation for two cities. *J. Appl. Meteorol. Climatol.* **47**: 1038–1060, doi: 10.1175/2007JAMC1597.1.

Park S-B, Kwak K-H, Han B-S, Ganbat G, Lee H, Seo JM, Lee S-H, Baik J-J. 2015. Measurements of turbulent flow and ozone at rooftop and sidewalk sites in a high-rise building area. *SOLA* **11**: 1–4, doi: 10.2151/sola.2015-001.

Porson A, Clark PA, Harman IN, Best MJ, Belcher SE. 2010. Implementation of a new urban energy budget scheme in the MetUM. Part I: Description and idealized simulations. *Q. J. R. Meteorol. Soc.* **136**: 1514–1529, doi: 10.1002/qj.668.

Rowley FB, Algren AB, Blackshaw JL. 1930. Surface conductances as affected by air velocity, temperature and character of surface. *ASHRAE Trans.* **36**: 429–446.

Ryu Y-H, Baik J-J. 2013. Daytime local circulations and their interactions in the Seoul metropolitan area. *J. Appl. Meteorol. Climatol.* **52**: 784–801, doi: 10.1175/JAMC-D-12-0157.1.

Ryu Y-H, Baik J-J, Lee S-H. 2011. A new single-layer urban canopy model for use in mesoscale atmospheric models. *J. Appl. Meteorol. Climatol.* **50**: 1773–1794, doi: 10.1175/2011JAMC2665.1.

Ryu Y-H, Bou-Zeid E, Wang Z-H, Smith JA. 2015. Realistic representation of trees in an urban canopy model. *Boundary-Layer Meteorol.* **159**: 193–220, doi: 10.1007/s10546-015-0120-y.

Salamanca F, Martilli A. 2010. A new building energy model coupled with an urban canopy parameterization for urban climate simulations. Part II. Validation with one dimension off-line simulations. *Theor. Appl. Climatol.* **99**: 345–356, doi: 10.1007/s00704-009-0143-8.

Schneider A, Mertes CM, Tatem AJ, Tan B, Sulla-Menashe D, Graves SJ, Patel NN, Horton JA, Gaughan AE, Rollo JT, Schelly IH, Stevens FR, Dastur A. 2015. A new urban landscape in East-Southeast Asia, 2000–2010. *Environ. Res. Lett.* **10**: 034002, doi: 10.1088/1748-9326/10/3/034002.

Shashua-Bar L, Tsiros IX, Hoffman ME. 2010. A modeling study for evaluating passive cooling scenarios in urban streets with trees. Case study: Athens, Greece. *Build. Environ.* **45**: 2798–2807, doi: 10.1016/j.buildenv.2010.06.008.

Shin HH, Dudhia J. 2016. Evaluation of PBL parameterizations in WRF at subkilometer grid spacings: Turbulence statistics in the dry convection boundary layer. *Mon. Weather Rev.* **144**: 1161–1177, doi: 10.1175/MWR-D-15-0208.1.

Skamarock WC. 2004. Evaluating mesoscale NWP models using kinetic energy spectra. *Mon. Weather Rev.* **132**: 3019–3032, doi: 10.1175/MWR2830.1.

Skamarock WC, Klemp JB, Dudhia J, Gill DO, Barker DM, Duda MG, Hwang X-Y, Wang W, Powers JG. 2008. 'A description of the advanced research WRF version 3', Technical Note 475+STR. National Center for Atmospheric Research: Boulder, CO.

Souch CA, Souch C. 1993. The effect of trees on summertime below canopy urban climates: A case study, Bloomington, Indiana. *J. Arboric.* **19**: 303–312.

Stewart ID, Oke T. 2012. Local climate zones for urban temperature studies. *Bull. Am. Meteorol. Soc.* **93**: 1879–1900, doi: 10.1175/BAMS-D-11-00019.1.

Sugawara H, Hagishima A, Narita KI, Ogawa H, Yamano M. 2008. Temperature and wind distribution in an east-west oriented urban street canyon. *SOLA* **4**: 53–56, doi: 10.2151/sola.2008-014.

Swaid H. 1993. The role of radiative-convective interaction in creating the microclimate of urban street canyons. *Boundary-Layer Meteorol.* **64**: 231–259.

Taha H. 1997. Urban climates and heat islands: Albedo, evapotranspiration, and anthropogenic heat. *Energy Build.* **25**: 99–103, doi: 10.1016/S0378-7788(96)00999-1.

Theeuwes NE, Steeneveld GJ, Ronda RJ, Heusinkveld BG, van Hove LWA, Holtslag AAM. 2014. Seasonal dependence of the urban heat island on the street canyon aspect ratio. *Q. J. R. Meteorol. Soc.* **140**: 2107–2210, doi: 10.1002/qj.2289.

United Nations. 2012. 'World urbanization prospects: The 2011 revision. No. ESA/P/WP.224. United Nations Department of Economic and Social Affairs/ Population Division: New York, NY.

Wang Z-H, Bou-Zeid E, Smith JA. 2013. A coupled energy transport and hydrological model for urban canopies evaluated using a wireless sensor network. *Q. J. R. Meteorol. Soc.* **139**: 1643–1657, doi: 10.1002/qj.2032.

Wouters H, Demuzere M, De Ridder K, van Lipzig N. 2015. The impact of impervious water-storage parameterization on urban climate modeling. *Urban Clim.* **11**: 24–50, doi: 10.1016/j.uclim.2014.11.005.

Wyngaard J. 2004. Toward numerical modeling in the 'terra incognita'. *J. Atmos. Sci.* **61**: 1816–1826, doi: 10.1175/1520-0469(2004)061<1816:TNMITT>2.0.CO;2.

Yamada T. 1982. A numerical study of turbulent airflow in and above a forest canopy. *J. Meteorol. Soc. Jpn.* **60**: 439–454.

Yang J, Wang Z-H, Chen F, Miao S, Tewari M, Voogt JA, Myint S. 2015. Enhancing hydrologic modelling in the coupled Weather Research and Forecasting-urban modelling system. *Boundary-Layer Meteorol.* **155**: 87–109, doi: 10.1007/s10546-014-9991-6.

Zahumensky I. 2004. *Guidelines on Quality Control Procedures for Data from Automatic Weather Stations*. Geneva, Switzerland: World Meteorological Organization.

